



Multi-process herbicide transport in structured soil columns: Experiments and model analysis

J. Maximilian Köhne^{a,*}, Sigrid Köhne^a, Jirka Šimůnek^b

^a *Institute for Land Use, Faculty for Agricultural and Environmental Sciences, University of Rostock, Justus-von-Liebig-Weg 6, 18044 Rostock, Germany*

^b *University of California, Riverside, Department of Environmental Sciences, 900 University Avenue, A135 Bourns Hall, Riverside, CA 92521, United States*

Received 16 June 2005; received in revised form 12 December 2005; accepted 3 January 2006

Available online 21 February 2006

Abstract

Model predictions of pesticide transport in structured soils are complicated by multiple processes acting concurrently. In this study, the hydraulic, physical, and chemical nonequilibrium (HNE, PNE, and CNE, respectively) processes governing herbicide transport under variably saturated flow conditions were studied. Bromide (Br^-), isotoproturon (IPU, 3-(4-isopropylphenyl)-1,1-dimethylurea) and terbutylazine (TER, N^2 -tert-butyl-6-chloro- N^4 -ethyl-1,3,5-triazine-2,4-diamine) were applied to two soil columns. An aggregated Ap soil column and a macroporous, aggregated Ah soil column were irrigated at a rate of 1 cm h^{-1} for 3 h. Two more irrigations at the same rate and duration followed in weekly intervals. Nonlinear (Freundlich) equilibrium and two-site kinetic sorption parameters were determined for IPU and TER using batch experiments. The observed water flow and Br^- transport were inversely simulated using mobile-immobile (MIM), dual-permeability (DPM), and combined triple-porosity (DP-MIM) numerical models implemented in HYDRUS-1D, with improving correspondence between empirical data and model results. Using the estimated HNE and PNE parameters together with batch-test derived equilibrium sorption parameters, the preferential breakthrough of the weakly adsorbed IPU in the Ah soil could be reasonably well predicted with the DPM approach, whereas leaching of the strongly adsorbed TER was predicted less well. The transport of IPU and TER through the aggregated Ap soil could be described consistently only when HNE, PNE, and CNE were simultaneously accounted for using the DPM. Inverse parameter estimation suggested that two-site kinetic sorption in inter-aggregate flow paths was reduced as compared to within aggregates, and that large values for the first-order degradation rate were an artifact caused by irreversible sorption. Overall, our results should be helpful to enhance the understanding and

* Corresponding author.

E-mail addresses: max.koehne@uni-rostock.de (J.M. Köhne), sigrid.koehne@uni-rostock.de (S. Köhne), jiri.simunek@ucr.edu (J. Šimůnek).

modeling of multi-process pesticide transport through structured soils during variably saturated water flow.

© 2006 Elsevier B.V. All rights reserved.

Keywords: Pesticides; Preferential flow; Reactive transport; Physical nonequilibrium; Chemical nonequilibrium; Modeling; Dual-permeability; Triple-porosity; HYDRUS-1D

Abbreviations and notations

Acronyms

Br⁻ dissolved bromide
 BTC breakthrough curve
 CNE chemical nonequilibrium
 DPM dual-permeability model
 DP-MIM dual-permeability mobile–immobile model
 DP-KM dual-permeability kinetic model
E statistical measure: modified coefficient of agreement (Eq. (23))
 HNE hydraulic nonequilibrium
 IPU isoproturon
 MAE statistical measure: mean absolute deviation (Eq. (24))
 MIM mobile–immobile model
 PFP preferential flow path
 PNE physical nonequilibrium
 TER terbutylazine

Symbols

c (M L⁻³) solute concentration
D (L² T⁻¹) dispersion coefficient
*D*₀ (L² T⁻¹) diffusion coefficient
*f*_f (-) fraction of equilibrium sorption sites in the fracture pore region of the DP-KM, Eqs. (19a) and (20a), or factor to increase or decrease sorption in the fracture pore region of the DPM, Eq. (15a)
*f*_m (-) fraction of equilibrium sorption sites in the matrix of the DP-KM
*f*_{mo} (-) fraction of sorption sites in contact with the mobile region
 1 - *f*_{mo} (-) fraction of sorption sites in contact with the immobile region
h (L) pressure head
K (L T⁻¹) hydraulic conductivity
*K*_m (L T⁻¹) effective hydraulic conductivity of the matrix, Eq. (8)
*K*_s (L T⁻¹) saturated hydraulic conductivity
*k*_{fr} (M^{-β} L^{3β}) Freundlich distribution coefficient
M (-) number of data-sets
n (-) van Genuchten's (1980) soil hydraulic parameter
N (-) number of observations
O (-) experimental observation
q (L T⁻¹) volumetric water flux density

s ($M M^{-1}$)	adsorbed solute concentration
s_e ($M M^{-1}$)	adsorbed solute concentration associated with equilibrium sorption site fraction
s_k ($M M^{-1}$)	adsorbed concentration of solute associated with kinetic sorption site fraction
t (T)	time
v_j (–)	weighting factor for a particular data-set in the objective function, Eq. (21)
w_f (–)	volumetric fraction of the fracture pore system
w_{ij} (–)	weighting factor for individual data-points in the objective function
z (L)	vertical spatial coordinate
α (L^{-1})	van Genuchten's (1980) soil hydraulic parameter
β (–)	exponent of Freundlich sorption isotherm
λ (L)	dispersivity
μ (T^{-1})	first-order herbicide degradation constant in the liquid phase
θ ($L^3 L^{-3}$)	water content
θ_r ($L^3 L^{-3}$)	residual water content parameter in the van Genuchten's (1980) model
θ_s ($L^3 L^{-3}$)	saturated water content parameter in the van Genuchten's (1980) model
ρ ($M L^{-3}$)	bulk density
σ (–)	variance
τ (–)	exponent in the van Genuchten hydraulic conductivity function
ω_h ($L^{-1} T^{-1}$)	first-order water transfer rate coefficient
ω_p (T^{-1})	first-order solute transfer rate coefficient
ω_c (T^{-1})	first-order kinetic sorption rate coefficient
Γ_h (T^{-1})	first-order water transfer rate
Γ_p ($M L^{-3} T^{-1}$)	first-order solute transfer rate
Φ_c (–)	objective function

Subscripts

c	chemical nonequilibrium (in the kinetic sorption rate coefficient, ω_c)
e	equilibrium (in s_e , Eqs. (18a,b))
f	fracture pore region
h	hydraulic (in ω_h , Eqs. (5) and (7))
i	numbering index, $1 \leq i \leq n$, Eq. (21).
im	immobile region
j	numbering index, $1 \leq j \leq m$, Eq. (21).
k	kinetic (in s_k , Eqs. (18a,b))
m	matrix
mo	mobile region
p	physical nonequilibrium (in the solute transfer rate coefficient, ω_p)

1. Introduction

Pesticides are applied on arable land to prevent crop disease and to secure the crop production. Pesticide findings in surface and ground waters have raised public concern. Diffuse herbicide losses from agricultural fields generally dominate detections in ground and surface waters as compared to point sources such as accidental spills and leaks (USEPA, 1993).

Fine-textured soils containing clay minerals and organic matter may act as sorption filter against pesticide leaching. However, this filter is often perforated by soil structural elements such as biopores (earthworm burrows, decayed plant root channels) or mechanical shrinkage patterns (cracks or fractures). Through these preferential flow paths (PFP), up to a few percent of the surface-applied pesticide may be channeled below the root zone, particularly during rainstorm events soon after pesticide application (e.g., Flury, 1996; Klavivko et al., 2001).

Pesticide fate and transport in structured soils was studied in the past using experimental and modeling approaches. In batch experiments, pesticide sorption was investigated in terms of sorption isotherms, ad- and desorption hysteresis, and kinetic sorption (e.g., Berglof et al., 2003; Smith et al., 2003; Cooke et al., 2004). Kinetic sorption is a chemical nonequilibrium (CNE) process, where either the sorption reaction at the soil–solution interface or the diffusion to the sorption sites is slow. Transport experiments with structured soil columns demonstrated effects of preferential water flow on pesticide transport (e.g., Czapar et al., 1992; Meyer-Windel et al., 1999). Preferential flow and solute transport are characterized by hydraulic nonequilibrium (HNE) and physical nonequilibrium (PNE), i.e., by distinct local differences between flow velocities, water contents, pressure heads for HNE (Köhne and Mohanty, 2005) and by different advective solute transport velocities and concentrations for PNE (e.g., Vanderborght et al., 2002) across soil regions associated with different mobility. Furthermore, pesticide movement was also strongly affected by CNE (e.g., James and Rubin, 1979; Valocchi, 1985). To complicate the matter, PNE and CNE during transport may produce somewhat similar effects of limited pesticide sorption, and may act concurrently (e.g., Gamedainger et al., 1990; Selim et al., 1999).

Models that do not account for PNE cannot accurately describe observations of pesticide leaching through structured soils in the presence of preferential flow (Pennell et al., 1990; Parrish et al., 1992; Veeh et al., 1994). Accordingly, one line of solute transport model development focused on the description of PNE based on the two-region concept. Common two-region approaches include, among others, i) dual-porosity or mobile–immobile models (MIM) that assume either steady-state (e.g., van Genuchten and Wierenga, 1976) or transient (Šimůnek et al., 2003) water flow, and ii) two-flow domain or dual-permeability models (DPM) that also assume either steady-state (Skopp et al., 1981; Ma and Selim, 1995) or transient (e.g., Gerke and van Genuchten, 1993; Jarvis, 1994) flow. These two-region approaches generally assume instantaneous reversible chemical sorption and identical sorption isotherms in both regions.

Another line of contaminant transport model development concentrated on CNE presuming that sorption to the soil solid phase is kinetic only (Valocchi, 1985), or supposing that sorption is characterized by simultaneous equilibrium and kinetic processes, where the sorbent in the soil can be divided into equilibrium (type-1) and kinetic (type-2) sites (e.g., van Genuchten and Wierenga, 1976; Cameron and Klute, 1977). Such two-site sorption models were shown to apply for many pesticides (e.g., Brusseau and Rao, 1989; Ball and Roberts, 1991).

Finally, coupled PNE–CNE transport models were developed. For instance, Brusseau et al. (1989) proposed a model where PNE (two-region MIM) and CNE (two-site sorption model) transport descriptions were combined. Wagenet and Chen (1998) combined models of single-rate or gamma-distributed multi-rate sorption with MIM. The resulting PNE–CNE models gave improved descriptions of atrazine breakthrough curves (BTCs) from column experiments, particularly for the multi-rate sorption model (Wagenet and Chen, 1998). Ma and Selim (1998) combined kinetic one-site or multiple-site adsorption models with MIM and obtained better agreement with measured metolachlor and chromium breakthrough curves. Selim et al. (1999)

linked a second-order two-site model with a MIM and yielded improved description of metolachlor transport in soil columns. Most recently, DPM were coupled with the two-site kinetic sorption model (Ray et al., 2004; Pot et al., 2005), which resulted into excellent simulations of IPU and metribuzin transport in structured soil columns (Pot et al., 2005).

However, coupled PNE–CNE approaches are generally limited to steady-state water flow and cannot account for natural transient flow conditions. On the other hand, transient-flow DPM with their simple description of equilibrium sorption may not realistically describe pesticide transport in natural soils (Dubus and Brown, 2002). Contrary to model assumptions, differing sorption properties were measured for PFPs and soil matrix. Organic linings of earthworm burrows were found to increase the total organic carbon content and Freundlich distribution coefficient, and degradation constant, as compared to the adjacent bulk soil matrix (Stehouwer et al., 1993, 1994; Mallawatantri et al., 1996). Fracture coatings may not only result in different hydraulic conductivity (Gerke and Köhne, 2002) and diffusion properties (Chen et al., 1997; Köhne et al., 2002a), but may also alter herbicide sorption (Celis et al., 1997).

The overall objective of this work was to identify and simulate the processes governing the leaching of two common herbicides with contrasting sorption properties, isoproturon and terbuthylazine, in aggregated and macroporous soil columns during transient flow. For this end, the MIM, DPM, and triple-porosity (DP-MIM) approaches within modified HYDRUS-1D (Šimůnek et al., 2003; Pot et al., 2005), were here further extended for variably saturated, transient flow conditions. Specific objectives were to analyze (i) if model parameters obtained from inverse analysis of transient water flow and Br^- transport and from equilibrium or kinetic batch herbicide sorption experiments can be applied in the forward simulation of herbicide transport during variably saturated flow, (ii) if the experimental data were sufficient to identify the governing HNE–PNE–CNE processes and corresponding model parameters and (iii) if there were differences in herbicide sorption between the PFP and the matrix domains.

2. Material and methods

Part of the experimental data, i.e. Br^- and isoproturon transport in the Ap and Ah columns, was published by the second author (Meyer-Windel et al., 1999). Since the terbuthylazine transport data and the equilibrium and kinetic sorption batch experiments for terbuthylazine and isoproturon have not yet been published, the experimental procedure is described below.

2.1. Soil description

Undisturbed soil columns (14.7 cm diameter, and 15 cm long) were excavated manually from a loamy (Ap) and a sandy (Ah) topsoil (Meyer-Windel et al., 1999). Additionally, bulk soil samples were taken from the same horizons. The soil from the Ap horizon was ploughed every fall and had a subangular aggregate structure. The sandy Ah soil was not tilled for four years prior to sampling and the Ah soil column contained a continuous earthworm burrow. Table 1 gives an overview of selected physical and chemical characteristics of the two soil horizons.

2.2. Batch studies: equilibrium and kinetic herbicide sorption

Equilibrium and time dependent (kinetic) sorption of the phenylurea herbicide isoproturon (IPU, 3-(4-isopropylphenyl)-1,1-dimethylurea) and the triazine herbicide terbuthylazine (TER, N^2 -tert-butyl-6-chloro- N^4 -ethyl-1,3,5-triazine-2,4-diamine) as commercial products [®]Arelon

Table 1
Selected physical and chemical properties of the Ap and Ah horizons

Horizon	Depth (m)	Clay (%)	Silt (%)	Sand (%)	ρ (g cm ⁻³)	Structure	C_{org} (%)	pH
Ap	0–0.3	2.3	43.8	54	1.37	Subangular to crumb	1.83	6.7
Ah	0–0.25	9.2	19	71.7	1.46	Crumb, earthworm burrows	1.55	6.1

Equivalent particle diameter (in 10⁻⁶ m): Clay, <2; Silt, 2–63; Sand, >63–2000. The pH was measured in 0.01 M CaCl₂ solution. ρ =bulk density, C_{org} =organic carbon.

and ®Gardoprim were tested on soil materials from the Ah and Ap horizons. The soil material was air dried and passed through a 2-mm sieve. Adsorption rates were quantified using 0.01 M CaCl₂ solutions that carried 0.2 mg L⁻¹ of either TER or IPU. Duplicate samples of 5 g sterile soil and 25 mL herbicide solution were shaken overhead in inert OAK-Ridge centrifuge tubes for 0.016, 0.33, 0.66, 1.33, 3, 9, 12, 24, 48, and 72 h. After shaking, the tubes were rotated in a centrifuge at 4600 ×g for 30 min whereupon 20 mL of the supernatant solution were removed and stored at 4 °C until chemical analysis. The difference between concentrations before and after shaking was attributed to sorption.

Additionally, we followed Streck et al. (1995) who showed that for organic pesticides undergoing a two-site (fast and slow) sorption process, both equilibrium sorption constants and sorption rates can be derived by fitting the two-site sorption model to data of hysteretic ad- and desorption isotherms. Ad- and desorption equilibrium isotherms were measured using a 0.01 M CaCl₂ solution containing 0.05 (0.05), 0.1 (0.1), 0.5 (0.5), 2 (2) and 10 (5) mg L⁻¹ IPU (TER). To obtain an adsorption isotherm, duplicate samples of 5 g soil and 25 mL herbicide solution were equilibrated by overhead shaking for 24 h. Again tubes were rotated and solution was withdrawn and stored as described above. Then desorption isotherms were established by adding 20 mL of herbicide-free CaCl₂ solution to the soil-solution remainder of the adsorption procedure. Again tubes were shaken (24 h), rotated, and solution was removed and stored as described previously. The desorption procedure was repeated three more times. Thus, the adsorption–desorption procedure yielded 1 adsorption and 4 desorption isotherms per herbicide-soil combination. The adsorption isotherms were calculated from sorbed concentrations (s) as the difference in the herbicide concentrations before (c_0) and after equilibration (c_e), multiplied with the solution/soil ratio ($s=5(s_0-c_e)$). For the i th-desorption isotherm of a herbicide-soil combination ($i=1, 2, 3, 4$; $i=0$ is for adsorption), the sorbed concentrations (s_i) were calculated using the corresponding measured equilibrium concentration ($c_{e,i}$), and the previously sorbed (s_{i-1}) and dissolved ($c_{e,i-1}$) concentrations, as $s_i=s_{i-1}-[5(c_{e,i}-c_{e,i-1})]$.

The two-site sorption concept (e.g., van Genuchten and Wagenet, 1989) was assumed to represent the solute concentration in the solid phase, s , to be associated with two different kinds of sorption sites

$$s = s_e + s_k \quad (1)$$

where s_e (MM⁻¹) denotes the adsorbed concentration of a solute in instantaneous equilibrium with the fraction of equilibrium sorption sites, and s_k (MM⁻¹) correspondingly symbolizes the remaining concentration of a solute attached to the solid phase by a slower, time-dependent process. The first-order rate equation for kinetic solute sorption at the type-2 sites is written as

$$\frac{\partial s_k}{\partial t} = \omega_c [(1-f)k_{\text{fr}}c^\beta - s_k] \quad (2)$$

where ω_c is a first-order sorption rate constant [T^{-1}], f is the fraction of equilibrium sorption sites [–], k_{fr} is the Freundlich distribution coefficient [$M^{-\beta} L^{3\beta}$], and β is the exponent of the Freundlich isotherm model [–] which reads $s = k_{fr} c^\beta$. Four parameters of the two-site sorption model (k_{fr} , β , ω_c , f) were estimated using a Levenberg–Marquardt based optimization routine (Streck et al., 1995) to minimize the sum of squared deviations between measured and calculated hysteretic ad- and desorption isotherms.

2.3. Transport studies

Transport experiments were conducted with natural (undisturbed, structured) soil columns under natural (transient, variably saturated) water flow conditions. We used the soil column set-up as described by Rambow and Lennartz (1993). The setup was placed in an air conditioned lab (ambient temperature of $20\text{ }^\circ\text{C} \pm 2$). At the top column boundary, a rainfall simulator with adjustable sprinkling rate was installed. At the bottom column boundary, constant suction of 3 kPa was applied using a vacuum pump. Three magnetic valves per column outlet controlled the effluent collection while maintaining the constant applied suction at the lower boundary. Tensiometers (0.5-cm diam.) were inserted into the soil columns at depths of 2.8 and 12.8 cm for pressure head measurements. Each column was placed on a balance to register changes of column mass, from which changes in the total volumetric soil water content were calculated based on the known column volume. A data-logging and control unit automatically controlled the column set-up and collected data.

Initial water contents of each column were determined as the difference between initial and oven-dry soil column mass (after the experiment), divided by the soil core volume, to be 0.320 (0.316) $\text{cm}^3 \text{ cm}^{-3}$ for the Ap (Ah) soil. The transport experiment was started by applying 0.005 L (0.029 cm) of a solution of Br^- , IPU, and TER during 20 min to the surface of both the Ap and Ah column. For Ap (Ah), the application contained 1010 (1034) $\text{mg L}^{-1} \text{ Br}^-$, and a whitish suspension of 254 (336) mg L^{-1} IPU and 290 (314) mg L^{-1} TER. The solubility of IPU in $^{\text{®}}$ Arelon (TER in $^{\text{®}}$ Gardoprim 500) is 170 mg L^{-1} (8.5 mg L^{-1}) at $20\text{ }^\circ\text{C}$ (IVA, 1990). The applied doses of active ingredients (0.8 – 1 kg AI/ha) and concentrations above solubility were chosen to represent typical agricultural application for crop protection, as done previously in column experiments (e.g., Roulier and Jarvis, 2003a). Starting 25 min after the application, a 3-cm (0.5 L) pulse of rain was applied at an intensity of 24 cm d^{-1} . Based on solubility and applied irrigation rate, IPU and TER were completely dissolved after 3 min and 1 h of the first irrigation, respectively. In weekly intervals, two (Ah: three) more rainfall events of the same depth and intensity were applied. An average evaporation of 0.3 cm d^{-1} over the experiment was estimated to be equal to inflow minus outflow minus change in column mass. Column effluent was continuously collected in 0.016 to 0.018 L samples by a fraction collector. Samples were stored at $4\text{ }^\circ\text{C}$ until Br^- and herbicide analysis.

2.4. Chemical analysis

Chemical analyses for Br^- were performed using an ion chromatography system with conductivity detector and for herbicides were done with on-line solid phase extraction (SPE) and reversed phase HPLC/UV–VIS spectroscopy. The detection limits were 0.2 mg L^{-1} for Br^- and 0.005 mg L^{-1} for herbicides in the extracted samples. Details about the chemical analysis procedures can be found in Meyer-Windel (1998).

2.5. Hydraulic nonequilibrium (HNE) water flow models

2.5.1. Mobile-immobile model, MIM

The MIM approach assumes that the soil water content, θ , is partitioned into a mobile region water content, θ_{mo} [L^3L^{-3}], and an immobile region water content, θ_{im} [L^3L^{-3}] (van Genuchten and Wierenga, 1976):

$$\theta = \theta_{\text{mo}} + \theta_{\text{im}} \quad (3)$$

One-dimensional transient water flow in the mobile region is described with the Richards' equation, while a source/sink term accounts for water exchange with the immobile region (Šimůnek et al., 2001, 2003):

$$\frac{\partial \theta_{\text{mo}}}{\partial t} = \frac{\partial}{\partial z} \left[K(h_{\text{mo}}) \left(\frac{\partial h_{\text{mo}}}{\partial z} - 1 \right) \right] - \Gamma_{\text{h}}^{\text{MIM}}$$

$$\frac{\partial \theta_{\text{im}}}{\partial t} = \Gamma_{\text{h}}^{\text{MIM}} \quad (4)$$

where t [T] is time, z [L] is the vertical distance positive downward, K [L T^{-1}] is the hydraulic conductivity as a function of the pressure head in the mobile region, h_{mo} [L], and $\Gamma_{\text{h}}^{\text{MIM}}$ [T^{-1}] is the water transfer rate between the mobile and immobile regions (subscript h refers to HNE):

$$\Gamma_{\text{h}}^{\text{MIM}} = \omega_{\text{h}} [h_{\text{mo}} - h_{\text{im}}] \quad (5)$$

where ω_{h} [$\text{L}^{-1}\text{T}^{-1}$] is a first-order water transfer rate coefficient.

2.5.2. Dual-permeability model, DPM

In the DPM, water flow in the preferential flow paths or fractures (subscript f) and in the soil matrix (subscript m) are described with Richards' equations (Gerke and van Genuchten, 1993):

$$\frac{\partial \theta_{\text{f}}}{\partial t} = \frac{\partial}{\partial z} \left(K_{\text{f}} \frac{\partial h_{\text{f}}}{\partial z} - K_{\text{f}} \right) - \frac{\Gamma_{\text{h}}^{\text{DPM}}}{w_{\text{f}}} \quad (6a)$$

$$\frac{\partial \theta_{\text{m}}}{\partial t} = \frac{\partial}{\partial z} \left(K_{\text{m}} \frac{\partial h_{\text{m}}}{\partial z} - K_{\text{m}} \right) + \frac{\Gamma_{\text{h}}^{\text{DPM}}}{1 - w_{\text{f}}} \quad (6b)$$

where K_{m} , θ_{m} , and K_{f} , θ_{f} are the local hydraulic conductivity and water content of the matrix and fracture pore system (e.g., Köhne et al., 2002b), respectively (as opposed to global state variables θ_{mo} , θ_{im} and K in Eq. (4) related to the total soil volume), w_{f} is the dimensionless volume fraction of the fracture pore system for converting local to global variables (e.g., $w_{\text{f}}\theta_{\text{f}}$), and $\Gamma_{\text{h}}^{\text{DPM}}$ [T^{-1}] is the rate of water exchange between the fracture and matrix regions:

$$\Gamma_{\text{h}}^{\text{DPM}} = \omega_{\text{h}} \bar{K}_{\text{m}} (h_{\text{f}} - h_{\text{m}}) \quad (7)$$

where ω_{h} [$\text{L}^{-1}\text{T}^{-1}$] is a first-order water transfer rate coefficient, and the effective hydraulic conductivity of the matrix, \bar{K}_{m} [L T^{-1}], was averaged in terms of h_{f} and h_{m} as follows

$$\bar{K}_{\text{m}} = (K_{\text{m}}(h_{\text{f}}) + K_{\text{m}}(h_{\text{m}})). \quad (8)$$

2.6. Physical nonequilibrium (PNE) solute transport models

2.6.1. Mobile–immobile model, MIM

The MIM describes solute transport at variably saturated water flow subject to instantaneous reversible sorption and first-order degradation in the liquid phase of each region as follows

$$\frac{\partial \theta_{\text{mo}} c_{\text{mo}}}{\partial t} + \frac{\partial f_{\text{mo}} \rho s_{\text{mo}}}{\partial t} = \frac{\partial}{\partial z} \left(\theta_{\text{mo}} D_{\text{mo}} \frac{\partial c_{\text{mo}}}{\partial z} \right) - \frac{\partial q_{\text{mo}} c_{\text{mo}}}{\partial z} - \mu \theta_{\text{mo}} c_{\text{mo}} - \Gamma_{\text{p}}^{\text{MIM}} \quad (9a)$$

$$\frac{\partial \theta_{\text{im}} c_{\text{im}}}{\partial t} + \frac{\partial (1 - f_{\text{mo}}) \rho s_{\text{im}}}{\partial t} = -\mu \theta_{\text{im}} c_{\text{im}} + \Gamma_{\text{p}}^{\text{MIM}} \quad (9b)$$

where for the mobile (subscript mo) region, c_{mo} is the solute concentration [M L^{-3}], D_{mo} is the dispersion coefficient [$\text{L}^2 \text{T}^{-1}$], q_{mo} is the volumetric flux density [L T^{-1}], f_{mo} is the fraction of sorption sites in the mobile region [–], $\Gamma_{\text{p}}^{\text{MIM}}$ is the solute transfer rate between the two regions (subscript p refers to PNE) [$\text{M L}^{-3} \text{T}^{-1}$], and μ [T^{-1}] represents the first-order rate coefficient for degradation in the liquid phase. Furthermore, c_{im} is the solute concentration in the immobile region [M L^{-3}], and s_{mo} and s_{im} are the adsorbed solute concentrations [MM^{-1}] in the mobile and immobile regions, respectively, which were calculated using Freundlich equations:

$$s_{\text{mo}} = k_{\text{fr}} c_{\text{mo}}^{\beta} \quad (10a)$$

$$s_{\text{im}} = k_{\text{fr}} c_{\text{im}}^{\beta} \quad (10b)$$

where k_{fr} is the Freundlich distribution coefficient [$\text{L}^{3\beta} \text{M}^{-\beta}$], and β is the Freundlich model exponent [–]. The dispersion coefficient in the mobile domain, D_{mo} , was described with the following equation:

$$\theta_{\text{mo}} D_{\text{mo}} = \theta_{\text{mo}} D_0 \frac{\theta_{\text{mo}}^{7/3}}{\theta_{\text{s,mo}}^2} + \lambda_{\text{mo}} |q_{\text{mo}}| \quad (11)$$

where D_0 is the molecular diffusion [$\text{L}^2 \text{T}^{-1}$], λ_{mo} signifies the dispersivity in the mobile region [L], and $\theta_{\text{s,mo}}$ denotes the saturated water content in the mobile region. The rate of solute mass transfer between the mobile and immobile regions, $\Gamma_{\text{p}}^{\text{MIM}}$, is given by (Šimůnek et al., 2003):

$$\Gamma_{\text{p}}^{\text{MIM}} = \omega_{\text{p}}^{\text{MIM}} (c_{\text{mo}} - c_{\text{im}}) + \Gamma_{\text{h}}^{\text{MIM}} c^* \quad (12)$$

where c^* is equal to c_{mo} for $\Gamma_{\text{w}} > 0$ and c_{im} for $\Gamma_{\text{w}} < 0$, and $\omega_{\text{p}}^{\text{MIM}}$ is the constant first-order (PNE) diffusive solute mass transfer coefficient [T^{-1}].

2.6.2. Dual-permeability model, DPM

Solute transport in the fracture (subscript f) and matrix (subscript m) pore regions of the DPM were described with convection–dispersion equations (Gerke and van Genuchten, 1993):

$$\frac{\partial \theta_{\text{f}} c_{\text{f}}}{\partial t} + \frac{\partial \rho s_{\text{f}}}{\partial t} = \frac{\partial}{\partial z} \left(\theta_{\text{f}} D_{\text{f}} \frac{\partial c_{\text{f}}}{\partial z} \right) - \frac{\partial q_{\text{f}} c_{\text{f}}}{\partial z} - \mu \theta_{\text{f}} c_{\text{f}} - \frac{\Gamma_{\text{p}}^{\text{DPM}}}{w_{\text{f}}} \quad (13a)$$

$$\frac{\partial \theta_{\text{m}} c_{\text{m}}}{\partial t} + \frac{\partial \rho s_{\text{m}}}{\partial t} = \frac{\partial}{\partial z} \left(\theta_{\text{m}} D_{\text{m}} \frac{\partial c_{\text{m}}}{\partial z} \right) - \frac{\partial q_{\text{m}} c_{\text{m}}}{\partial z} - \mu \theta_{\text{m}} c_{\text{m}} + \frac{\Gamma_{\text{p}}^{\text{DPM}}}{1 - w_{\text{f}}} \quad (13b)$$

where for the fracture and matrix regions, c is the solute concentration [$M L^{-3}$], D is the dispersion coefficient [$L^2 T^{-1}$] which was described with an equation analogous to (11), q is the volumetric flux density [$L T^{-1}$], s is the adsorbed concentration [MM^{-v1}], and solute transfer Γ_p^{DPM} [$M L^{-3}T^{-1}$] is calculated as follows

$$\Gamma_p^{DPM} = \theta_m \omega_p^{DPM} \frac{\theta_m^{7/3}}{\theta_{s,m}^2} (1 - w_f)(c_f - c_m) + \Gamma_h^{DPM} c^* \quad (14)$$

where ω_p^{DPM} is a first-order diffusive solute mass transfer coefficient [T^{-1}], c^* is equal to c_f for $\Gamma_h^{DPM} > 0$ and c_m for $\Gamma_h^{DPM} < 0$, and the adsorbed concentrations in the fracture and matrix regions, s_f and s_m [MM^{-1}], were calculated as

$$s_f = f_f k_{fr} c_f^\beta \quad (15a)$$

$$s_m = k_{fr} c_m^\beta \quad (15b)$$

where f_f is an empirical factor [–] used to increase ($f_f > 1$) or decrease ($f_f < 1$) sorption in the fracture pore region.

2.6.3. Dual-permeability mobile-immobile model: DP-MIM

The DPM solute transport model described in Section 2.6.2 was, following Pot et al. (2005), extended into a triple-porosity model by assuming that the matrix water content, θ_m , can be further partitioned into mobile and immobile fractions similarly as in Eq. (3):

$$\theta_m = \theta_{mo} + \theta_{im}. \quad (16)$$

In the DP-MIM, solute transport in the fractures was described using Eq. (13a), while transport in the matrix was described using Eqs. (17a,b) with first-order diffusive solute transfer between the mobile and immobile matrix regions, and assuming time-variable θ_{mo} and constant θ_{im} :

$$\frac{\partial \theta_{mo} c_{mo}}{\partial t} + \frac{\partial \rho f_{mo} s_{mo}}{\partial t} = \frac{\partial}{\partial z} \left(\theta_{mo} D_{mo} \frac{\partial c_{mo}}{\partial z} \right) - \frac{\partial q_{mo} c_{mo}}{\partial z} - \theta_{mo} \mu c_{mo} + \frac{\Gamma_p^{DPM}}{1 - w_f} - \omega_p^{MIM} (c_{mo} - c_{im}) \quad (17a)$$

$$\theta_{im} \frac{\partial c_{im}}{\partial t} + \frac{\partial \rho (1 - f_{mo}) s_{im}}{\partial t} = \omega_p^{MIM} (c_{mo} - c_{im}) - \theta_{im} \mu c_{im} \quad (17b)$$

where s_{mo} and s_{im} were described with Freundlich Eqs. (10a) and (10b). In DP-MIM, f_{mo} is the fraction of sorption sites in the mobile region of the matrix domain [–].

2.7. Physical and chemical nonequilibrium solute transport model

2.7.1. Dual-permeability kinetic sorption transport model: DP-KM

In analogy to the two-site kinetic sorption model for bulk soil (Eqs. (1) and (2)), the adsorbed solute concentrations in the fracture pore system, s_f , and the matrix pore system, s_m , of the DP-KM were partitioned into equilibrium and rate-limited sorption sites

$$s_f = s_{e,f} + s_{k,f} \quad (18a)$$

$$s_m = s_{e,m} + s_{k,m} \quad (18b)$$

where for fracture (subscript f) and matrix (subscript m) domains, s_e (MM^{-1}) denotes the adsorbed solute concentration at equilibrium (type-1) sorption sites, and s_k (MM^{-1}) symbolizes the remaining adsorbed concentration of a solute attached to kinetic (type-2) sites of the solid phase assuming the following first-order rate equations (Pot et al., 2005):

$$\frac{\partial s_{k,f}}{\partial t} = \omega_{c,f} \left[(1 - f_f) k_{f,f} c_f^\beta - s_{k,f} \right] \quad (19a)$$

$$\frac{\partial s_{k,m}}{\partial t} = \omega_{c,m} \left[(1 - f_m) k_{f,m} c_m^\beta - s_{k,m} \right] \quad (19b)$$

where for fracture (subscript f) and matrix (subscript m) domains, $\omega_{c,f}$ and $\omega_{c,m}$ are first-order sorption rate constants [T^{-1}] and f_f and f_m are the fractions of equilibrium sorption sites [–].

The DP-KM approach describes solute transport at concurrent PNE and CNE conditions accounting for two-site kinetic reversible nonlinear sorption as follows:

$$\frac{\partial \theta_f c_f}{\partial t} + \frac{\partial \rho s_f}{\partial t} = \frac{\partial}{\partial z} \left(\theta_f D_f \frac{\partial c_f}{\partial z} \right) - \frac{\partial q_f c_f}{\partial z} - \mu \theta_f c_f - \frac{\Gamma_P^{\text{DPM}}}{w_f} - \rho \omega_{c,f} \left[(1 - f_f) k_{f,f} c_f^\beta - s_{k,f} \right] \quad (20a)$$

$$\frac{\partial \theta_m c_m}{\partial t} + \frac{\partial \rho s_m}{\partial t} = \frac{\partial}{\partial z} \left(\theta_m D_m \frac{\partial c_m}{\partial z} \right) - \frac{\partial q_m c_m}{\partial z} - \mu \theta_m c_m + \frac{\Gamma_P^{\text{DPM}}}{(1 - w_f)} - \rho \omega_{c,m} \left[(1 - f_m) k_{f,m} c_m^\beta - s_{k,m} \right]. \quad (20b)$$

A model somewhat similar to the DP-KM, although assuming linear adsorption isotherms, was recently presented by Ray et al. (2004).

2.8. Model parameter estimation

Model approaches in this study were parameter demanding, although to different extents (Table 2). To reduce the number of unknowns, some parameters were always fixed as follows. The parameter τ was set equal to 0.5 (Mualem, 1976). The parameters $\theta_{\text{mo},r}$ and $\theta_{\text{im},r}$ (MIM) and $\theta_{\text{m},r}$ and $\theta_{f,r}$ (DPM) were set to zero, which is consistent with zero θ_r values fitted to water retention and hydraulic conductivity data for the Ap and Ah soil columns (Meyer-Windel, 1998). The diffusion coefficient, D_0 , was calculated for Br^- ($1.797 \text{ cm}^2 \text{ d}^{-1}$) and for herbicides ($0.7 \text{ cm}^2 \text{ d}^{-1}$) according to Atkins (1990). Using dye tracer experiments with columns taken from the same soil horizons (Köhne, 1999), w_f was set equal to average values of dye coverage (Ap: $w_f=0.2$; Ah: $w_f=0.05$). Similarly, λ_m (0.5 cm) was derived from Br^- transport experiments performed with the Ap and Ah soil columns at unsaturated (-3 kPa) steady-state flow conditions (Meyer-Windel, 1998). In forward herbicide transport simulations, additional parameters were fixed. The parameter f_{mo} in the MIM and DP-MIM was assumed to be equal to $\theta_{\text{mo},s}/\theta_s$, whereas for DP-KM, f_f and f_m were assumed to be equal to f as determined in the batch test for total soil (Table 3). The sorption coefficients $k_{f,i}$, β , and ω_c were also fixed based on the batch experiments results and were as a first approximation assumed to be identical for different regions. In DPM and DP-MIM, the empirical factor f_f increasing or decreasing sorption in PFPs was set to its default value of one. The degradation coefficient μ at

Table 2
Model approaches with parameter requirements to describe transport of Br^- , IPU, and TER

Simulated process	Data	MIM	N	DPM	N	DP-MIM	N	DP-KM	N
Variably saturated transient water flow and water transfer between regions (HNE)	q, θ, h	$(\tau, \theta_{\text{mo,r}}, \theta_{\text{im,r}})^{\text{a}}$ $K_{\text{s}}, \theta_{\text{mo,s}}, \alpha_{\text{mo}},$ $n_{\text{mo}}, \theta_{\text{im,s}}, \alpha_{\text{im}},$ $n_{\text{im}}, \omega_{\text{h}}$	8	$(\theta_{\text{m,r}}, \tau_{\text{m}}, \theta_{\text{f,r}}, \tau_{\text{f}})^{\text{a}}$ $\theta_{\text{m,s}}, \alpha_{\text{m}}, n_{\text{m}}, K_{\text{m,s}},$ $\alpha_{\text{f}}, n_{\text{f}}, \theta_{\text{f,s}}, K_{\text{f,s}}, \omega_{\text{h}}$	9	$(\theta_{\text{mo,r}}, \tau_{\text{mo}}, \theta_{\text{f,r}}, \tau_{\text{f}})^{\text{a}}$ $\theta_{\text{mo,s}}, \alpha_{\text{mo}}, n_{\text{mo}}, K_{\text{mo,s}},$ $\theta_{\text{f,s}}, \alpha_{\text{f}}, n_{\text{f}}, K_{\text{f,s}}, \omega_{\text{h}}$	9	$(\theta_{\text{m,r}}, \tau_{\text{m}}, \theta_{\text{f,r}}, \tau_{\text{f}})^{\text{a}}$ $\theta_{\text{m,s}}, \alpha_{\text{m}}, n_{\text{m}}, K_{\text{m,s}},$ $\alpha_{\text{f}}, n_{\text{f}}, \theta_{\text{f,s}}, K_{\text{f,s}}, \omega_{\text{h}}$	9
+Convective–dispersive solute transport and solute transfer between regions (PNE)	$\text{Br}^- \text{BTC}$	$D_0^{\text{a}}, \lambda, \omega_{\text{p}}$	2	$(D_0, \lambda_{\text{m}})^{\text{a}}, \lambda_{\text{f}}, \omega_{\text{p}}$	2	$(D_0, \lambda_{\text{m}})^{\text{a}}, \theta_{\text{im}}, \lambda_{\text{f}},$ $\omega_{\text{p}}^{\text{DPM}}, \omega_{\text{p}}^{\text{MIM}}$	4	$(D_0, \lambda_{\text{m}})^{\text{a}}, \lambda_{\text{f}}, \omega_{\text{p}}$	2
+Nonlinear instantaneous sorption and decay	Batch tests IPU BTC	$(k_{\text{fb}}, \beta)^{\text{a}},$ f_{mo}, μ	2	$(k_{\text{fb}}, \beta)^{\text{a}}, f_{\text{f}}, \mu$	2	$(k_{\text{fb}}, \beta)^{\text{a}}, f_{\text{f}}, f_{\text{mo}}, \mu$	3		
+Kinetic sorption (CNE)	TER BTC	n.a.	n.a.		n.a.		n.a.	$(k_{\text{fb}}, \beta, f_{\text{m}}, \omega_{\text{c,m}})^{\text{a}},$ $f_{\text{f}}, \omega_{\text{c,f}}, \mu$	3

N = maximum number of fitted parameters, n.a. = not available.

^a Fixed at known or estimated value.

Table 3

Equilibrium (Ah-soil) and two-site kinetic (Ap-soil) sorption parameters of TER and IPU as obtained from batch tests

Soil-herbicide	k_{fr}	β	f	ω_c	R^2
Ap-TER	11.99	0.92	0.499	0.106	0.978
Ap-IPU	6.20	0.86	0.375	0.105	0.981
Ah-TER	3.73	0.92	–	–	0.999
Ah-IPU	1.33	0.89	–	–	0.993

20 °C was set to 0.046 d⁻¹ for IPU (half-life of 15 d) and 0.011 d⁻¹ for TER (half-life of 60 d), within the typical range of measured values (e.g., PerrinGanier et al., 1996; James et al., 1998; Walker et al., 2002).

The inverse parameter estimation was accomplished as follows. The water flow and conservative solute transport parameters (Table 2) were estimated using the experimental observations of cumulative water flow, pressure heads, water contents, and Br⁻ effluent concentrations. For herbicide transport simulations, the resulting hydraulic and transport parameter values were fixed, except that ω_p^{MIM} and ω_p^{DPM} were both multiplied by the ratio between D_0 of herbicides and Br⁻ (0.7/1.797). Most reactive transport parameters were fixed at their batch test values. Sorption parameters of the PFPs, and the degradation constant μ assumed to be similar in PFPs and matrix, were inversely estimated based on the measured herbicide effluent concentrations. For the various approaches, f_{mo} and f_f were estimated either alone or together with μ (DP-KM: also $\omega_{c,f}$ and f_f) (Table 2). Limiting the optimization of sorption properties to only the PFP region was done for three reasons: (i) PFP sorption properties are much more sensitive to herbicide transport during preferential flow than matrix sorption properties (Pot et al., 2005), (ii) the batch values mainly represented the matrix properties, since the matrix made up the bulk of soil, and (iii) the number of fitted parameters should be kept small.

Recently, an increasing number of theoretical and experimental studies reported that the dispersivity may not be a constant for a soil, but increases from conservative to (particularly nonlinearly) adsorbed solutes (e.g., Pot and Genty, 2005; Vanderborght et al., in press). To obtain a first impression of the potential significance of this effect for dispersion in preferential flow paths, λ_f was additionally fitted in few selected herbicide transport simulations.

The inverse parameter estimation was performed by Levenberg–Marquardt minimization of the objective function Φ (Šimůnek et al., 1998):

$$\Phi(\mathbf{b}) = \sum_{j=1}^m v_j \sum_{i=1}^n w_{ij} [O_j(z, t_i) - E_j(z, t_i, \mathbf{b})]^2 \quad (21)$$

where m represents the number of different measurement sets, n is the number of observations in a particular measurement set, $O_j(z, t_i)$ are observations at time t_i at location z , $E_j(z, t_i, \mathbf{b})$ are the corresponding estimated space–time variables for the vector \mathbf{b} of optimized parameters (Table 2), and v_j and w_{ij} are weighting factors associated with a particular measurement set or point, respectively. When simulating the Br⁻ transport experiment, $O_j(z, t_i)$ represented pressure heads in the mobile region at 2.8 and 12.8 cm depths, average soil column water contents (averaged over the column depth and over regions), cumulative water fluxes across the lower boundary, and effluent Br⁻ concentrations. For simulating the herbicide transport experiment, $O_j(z, t_i)$ included only herbicide concentrations in the effluent. The w_{ij} in Eq. (21) were set

equal to one assuming similar error variances within a particular measurement set. The v_j were calculated as (Šimůnek et al., 1998):

$$v_j = \frac{1}{N_j \sigma_j^2} \quad (22)$$

where σ_j^2 is the variance within the j -th measurement set, and N_j is the number of measurements within the set. The model performance was statistically evaluated using the dimensionless modified coefficient of efficiency, E (Legates and McCabe, 1999):

$$E = 1.0 - \frac{\sum_{i=1}^N [|E_j(z, t_i, \mathbf{b}) - O_j(z, t_i)|]}{\sum_{i=1}^N |O_j(z, t_i) - \bar{O}|} \quad (23)$$

where E varies between $-\infty$ to 1.0, with higher values indicating better agreement between the model and observations. A zero (negative, positive) value of E indicates that the model is statistically as good as (worse, better than) the mean (\bar{O}) to predict the data, with a unit value indicating perfect agreement between model and data. Compared to the coefficient of determination, R^2 , E is a more conservative and reliable statistical measure and is less sensitive to extreme values (Legates and McCabe, 1999). Throughout this study we will assume that $E > 0$ represents an “acceptable” simulation, while $E > 0.5$ represents a “good” simulation. Additionally, the mean absolute error (MAE) was calculated as

$$\text{MAE} = \frac{\sum_{i=1}^N [|E_j(z, t_i, \mathbf{b}) - O_j(z, t_i)|]}{N} \quad (24)$$

where MAE carries the same units as the observations. The observed and simulated herbicide and Br^- BTCs were compared using the relative and absolute error measures (23) and (24).

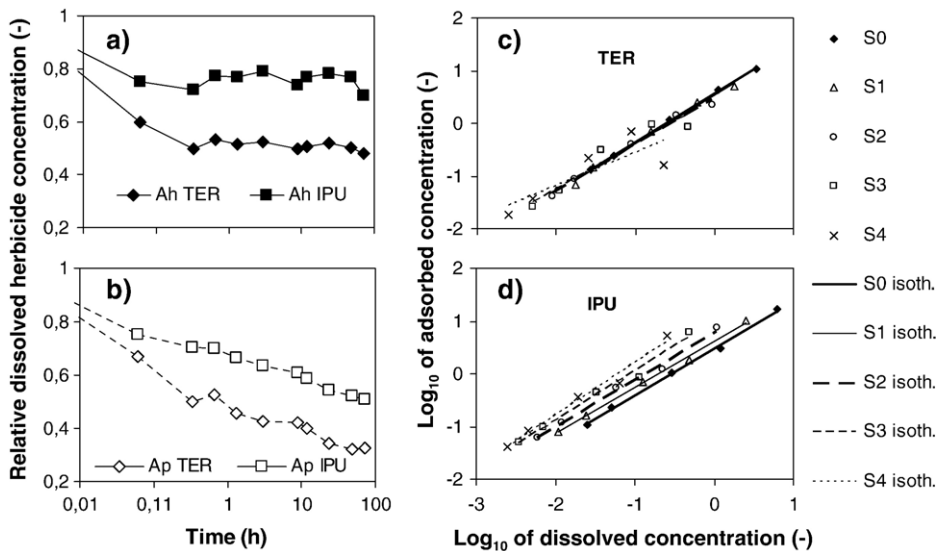


Fig. 1. Left: Measured time dependent sorption of IPU and TER with a) Ah soil and b) Ap soil, Right: data of a batch adsorption-(S0) experiment with 4 desorption (S1 to S4) steps, and corresponding fitted log-linear (Freundlich) isotherms, c) TER with the Ah soil material, and d) IPU with the Ap soil material.

For the water flow simulations, additionally an average soil hydraulic index of agreement, E_{hyd} , was calculated as the average over individual E values for outflow, water contents, and pressure heads (E_{outflow} , $E_{\text{water content}}$, $E_{\text{pressure head}}$):

$$E_{\text{hyd}} = \frac{E_{\text{outflow}} + E_{\text{water content}} + E_{\text{pressure head}}}{3} \quad (25)$$

The initial condition for water flow was represented by a hydrostatic pressure head profile linearly interpolated between measurements of tensiometers installed at 2.8 and 12.8 cm depth.

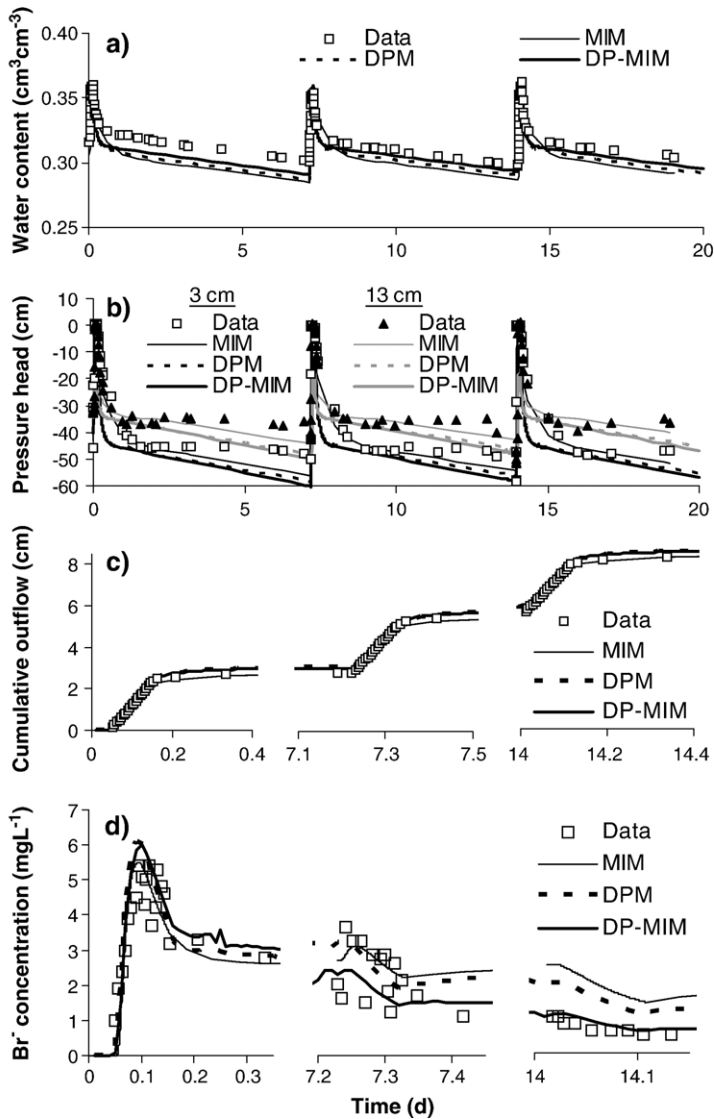


Fig. 2. Transient water flow and bromide (Br^-) transport data from the Ap-soil column, and corresponding model simulation results, a) bulk soil water contents, b) pressure heads at depths of 3 and 13 cm, c) cumulative outflow, and d) Br^- effluent concentrations.

The upper flow boundary condition was a variable flux-type condition equal to time-variable rates of irrigation (24 cm d^{-1}) and evaporation (0.3 cm d^{-1}) set according to the experimental conditions. For the lower boundary, an unsaturated seepage face at user-specified pressure heads of -6 kPa (Ah1) or -3 kPa (Ap1) was implemented in HYDRUS-1D. The initial Br^- and herbicide concentrations were set to zero. The upper and lower boundaries for solute transport were represented by specified flux and (zero) gradient conditions, respectively. The Br^- and herbicide concentrations (above solubility) were directly used in the small injection pulse (0.029 cm). In the following 25 min between injection and irrigation, the models internally simulated herbicide partitioning between soil solid and liquid phases according to the herbicide sorption and diffusion characteristics, after which the first water irrigation was applied. Neglecting herbicide dissolution kinetics in the boundary conditions should be negligible for IPU, which was applied in concentrations just slightly above solubility, and may have some (unknown) effect on TER transport simulations.

3. Results

3.1. Batch experiments

Fig. 1 shows selected results for the relative concentrations for the 4 herbicide-soil combinations during 72 h of adsorption (Fig. 1a,b) and ad- and desorption data (Fig. 1c,d). For the Ah soil material and both IPU and TER, the early drop from unity at time zero to more or less constant concentrations suggests instantaneous equilibrium adsorption (Fig. 1a). By contrast, for the Ap soil the almost log-linear decrease of dissolved concentrations of both herbicides over the entire 72 h (Fig. 1b) revealed rate-limited sorption. Accordingly, for the Ah material and the measured ad- and desorption data together with the isotherms obtained by linear regression of corresponding $5 \log c_{\text{eq}} - \log s$ -pairs were similar for ad- and desorption (Fig. 1c exemplarily shows Ah-TER), whereas the shift of sequential isotherms revealed hysteretic ad- and desorption relation for the Ap material and IPU or TER (Fig. 1d shows Ap-IPU as an example). Hence, instantaneous equilibrium sorption was assumed for both IPU and TER in the Ah soil, and values for k_{fr} and β were obtained by linear regression of the Freundlich isotherm to the corresponding double-logarithmic data of adsorbed versus dissolved concentrations (Table 3). For the Ap soil, the hysteretic sorption data were analyzed with the model of Streck et al. (1995) to obtain parameters of the two-site sorption model (Table 3) as described in Section 2.2.

3.2. Bromide transport

3.2.1. Ap soil column

The MIM, DPM, and DP-MIM inverse simulation results for water flow and Br^- transport in the Ap soil column are displayed in Fig. 2. We note that simulations were also performed with a single-domain model based on Richards' and convection-dispersion equations in HYDRUS-1D (Šimůnek et al., 1998) which failed to describe the observed Br^- concentrations (not shown). Observed bulk soil water contents varying between 0.3 and 0.36 (Fig. 2a), pressure heads between -60 and 0 cm (Fig. 2b), and cumulative outflow (Fig. 2c) for three intermittent irrigation events were more or less matched by all three models. The good agreement between model simulations and data was confirmed by the E_{hyd} values around 0.8 (Table 4).

Simulated Br^- BTCs were within fluctuations of measured concentrations up to 7.5 days (Fig. 2d). The early Br^- arrival with the first column effluent, the low Br^- peak of 5.5 mg L^{-1} ,

Table 4

Results for hydraulic and conservative solute transport parameters and corresponding (\pm) 95% confidence limits for the MIM, DPM, and DP-MIM, obtained by inverse estimation using water flow and Br⁻ concentration data for the Ah and Ap soil columns

Soil Model	Fracture and mobile region					Matrix and immobile region				Inter-region transfer			Goodness-of-fit E (MAE) E_{hyd} (mg L ⁻¹)
	θ_s^{\S} (cm ³ cm ⁻³)	α (cm ⁻¹)	n	K_s^{\S} (cm d ⁻¹)	λ (cm)	θ_s^{\parallel} (DPM– MIM: $\theta_{\text{mo}},\theta_{\text{im}}$) (cm ³ cm ⁻³)	α (cm ⁻¹)	n	K_s^{\parallel} (cm d ⁻¹)	Water	Bromide		
										ω_h (d ⁻¹)	ω_p^{MIM} (d ⁻¹)	ω_p^{DPM} (d ⁻¹)	
<i>Ap</i>													
MIM	0.148	0.0341	1.250	22.55	2.30	0.214	0.0162	2.000	n.a.	0.192	1.336	n.a.	0.43 (0.75)
	± 0.014	± 0.0020	± 0.042	± 0.90	± 0.89	± 0.014	± 0.0020	± 0.310		± 0.036	± 0.274		0.82
DPM	0.159	0.0312	1.301	61.62	2.75	0.212	0.0158	1.937	1.645	0.092	n.a.	5.35	0.48 (0.72)
	± 0.006	± 0.0006	± 0.028	± 2.98	± 0.40	± 0.008	± 0.0004	± 0.097	± 0.008	± 0.007		± 2.41	0.773
DP-MIM	0.162	0.0346	1.250	54.88	2.82	0.201; 0.0107	0.0133	1.951	1.475	0.156	0.021	2.55	0.55 (0.62)
	± 0.007	± 0.0025	± 0.039	± 1.43	± 0.46	± 0.008 ; 0.136	± 0.0005	± 0.156	± 0.138	± 0.021	± 0.020	± 4.52	0.82
<i>Ah</i>													
MIM	0.055	0.0461	1.348	34.57	2.34	0.313	0.0045	1.441	n.a.	0.010	0.774	n.a.	0.45 (0.92)
	± 0.006	± 0.0066	± 0.071	± 4.60	± 2.61	± 0.180	± 0.0028	± 0.323		± 0.008	± 0.348		0.82
DPM	0.050	0.0136	1.827	6.71	10 [#]	0.323	0.0011	1.362	2.741	0.009	n.a.	0.606	0.64 (0.72)
	± 0.003	± 0.0010	± 0.084	± 0.40	± 4.81	± 0.027	± 0.0000	± 0.039	± 0.218	± 0.001		± 0.252	0.81
DP-MIM	0.039	0.0140	2.188	6.88	0.42	0.110; 0.222	0.0016	1.250	2.154	0.010	0.074	3.62	0.82 (0.36)
	± 0.001	± 0.001	± 0.111	± 0.52	± 0.08	± 0.010 ; 0.031	± 0.0001	± 0.039	± 0.090	± 0.001	± 0.030	± 0.602	0.81

Fixed: $\theta_r=0$, $\lambda_m=0.5$ cm, $w_f=0.05$ (0.2) for Ah (Ap); n.a. — not available. [§]For DPM and DPM–MIM, divide value by $w_f=0.2$ (Ap) and $w_f=0.05$ (Ah) to obtain the corresponding local value for the fracture pore region, [¶]for DPM and DPM–MIM, divide by $(1-w_f)=0.8$ (Ap) and $(1-w_f)=0.95$ (Ah) to obtain the corresponding local value for the matrix, [#]at upper constraint.

corresponding to only 0.5% of the applied concentration of 1010 mg L^{-1} , and the shape of the Br^- BTC were delineated by all model approaches. The late-time low Br^- concentrations observed after two weeks could be only accurately captured using the DP-MIM (Fig. 2d). For the entire Br^- BTC with three irrigation events, the model performance was acceptable for MIM ($E=0.427$) and DPM (0.476), and was good for DPM–MIM (0.549). Mean absolute deviations, MAE, were below 0.75 mg L^{-1} and decreased in the order of MIM, DPM, and DPM–MIM (Table 4). For the Br^- BTC only up to 7.5 days, i.e., until outflow after the second irrigation event ceased, there was a good agreement between all models and data as reflected by $E > 0.5$. We conclude that for the Ap soil, the assumption of two pore domains was a suitable concept to describe Br^- leaching at HNE and PNE during the first two irrigation events. However, the late-time Br^- transport appeared to be dominated by diffusive transfer into the microporosity subdomain of the matrix acting as a sink for Br^- .

Table 4 furthermore shows estimated model parameters. First-order water and solute transfer parameters can only approximately be compared between two-flow region and MIM approaches as used in this study. For example, the fitted ω_h values controlling water and advective solute transfer are smaller in DPM and DP-MIM than in MIM, but estimated ω_h values in DPM and DP-MIM compensate for the effective matrix hydraulic conductivity, \bar{K}_m , in Eqs. (7) and (8). Similarly, in the solute transfer term (Eq. (14)) of DPM and DP-MIM, the fitted ω_p^{DPM} values are multiplied by the variable term $(\theta_m^{10/3}/\theta_{s,m}^2)(1-w_f) < 1$. The average reduction is compensated by the larger optimized values for ω_p^{DPM} as compared to ω_p^{DPM} in Eq. (12). In DP-MIM, where ω_p^{DPM} characterizes transfer between the fracture and matrix domains and ω_p^{MIM} between the mobile and immobile regions within the matrix, estimated values of ω_p^{MIM} and θ_{im} were so small (Table 4) that diffusive transfer between the mobile and immobile matrix regions only had a notable effect on simulated Br^- transport after prolonged time.

To facilitate inter-comparison between MIM and DPM approaches, the θ_s and K_s parameters in Table 4 are presented as global variables related to the total soil volume. In other words, θ_s and K_s values listed in Table 4 for DPM and DP-MIM were multiplied by w_f and $(1-w_f)$ for the fracture and matrix regions, respectively. Region-specific parameters did not differ much among different models, except that $w_f K_{s,f}$ for DPM and DP-MIM were almost 3 times as large as corresponding K_s values in the mobile region of MIM (Table 4). However, the fracture pore region in DPM and DP-MIM simulations did not wet up entirely ($h_f = -2 \text{ cm}$) during rainfall applications, while the mobile region in the MIM simulation fully saturated ($h_{mo} = 0 \text{ cm}$) as was experimentally observed. For DPM and DP-MIM, the inverse estimate of soil hydraulic conductivity ($K = w_f K_f + (1-w_f) K_m$) at $h = -2 \text{ cm}$ came to within 10% of the $K_{mo,s}$ value (22.55 cm d^{-1}) estimated with MIM. Similarly, the $w_f \theta_{f,s}$ values for DPM and DP-MIM were slightly larger than $\theta_{mo,s}$ for MIM (Table 4), whereas similar values were found for $\theta_{mo,s}$ and $w_f \theta_f$ at $h_f = -2 \text{ cm}$. Estimated $K_{f,s}$ values for DPM and DP-MIM were thus values extrapolated beyond the simulated pressure head range and are expected to be associated with large estimation errors.

These findings can be partly explained with the over-parameterization of DPM and DPM–MIM and may be used as an argument for always using a simpler approach (MIM) simultaneously with more complex approaches to cross-check the physical meaning of parameters obtained by inverse estimation. However, recognizing the overestimated $K_{s,f}$ values, DPM and DP-MIM can still be used in subsequent herbicide transport simulations.

3.2.2. Ah soil column

Experimental results for water flow and Br^- transport in the Ah column are shown in Fig. 3 together with corresponding model results, while estimated model parameters and statistical

measures are presented in Table 4. Pressure heads between -200 and 0 cm (Fig. 3a) and cumulative outflow (Fig. 3b) show the hydraulic response of the soil system to four irrigations and subsequent redistribution events. No water contents were measured for the Ah soil column. Simulations were in good agreement with hydraulic data (Fig. 3a,b) with $E_{\text{hyd}} > 0.8$ for all three models (Table 4).

The Br^- BTC had a highly left-skewed shape with the peak already encountered in the first percolate sample, and a higher peak concentration of 18 mg L^{-1} (2% of the applied concentration) than for the Ap soil column (Fig. 3c). This is again indicative of preferential flow with pronounced HNE and PNE. Similarly as for the Ap soil column, both MIM and DPM approximated the Br^- breakthrough well during the first week, while only the DP-MIM

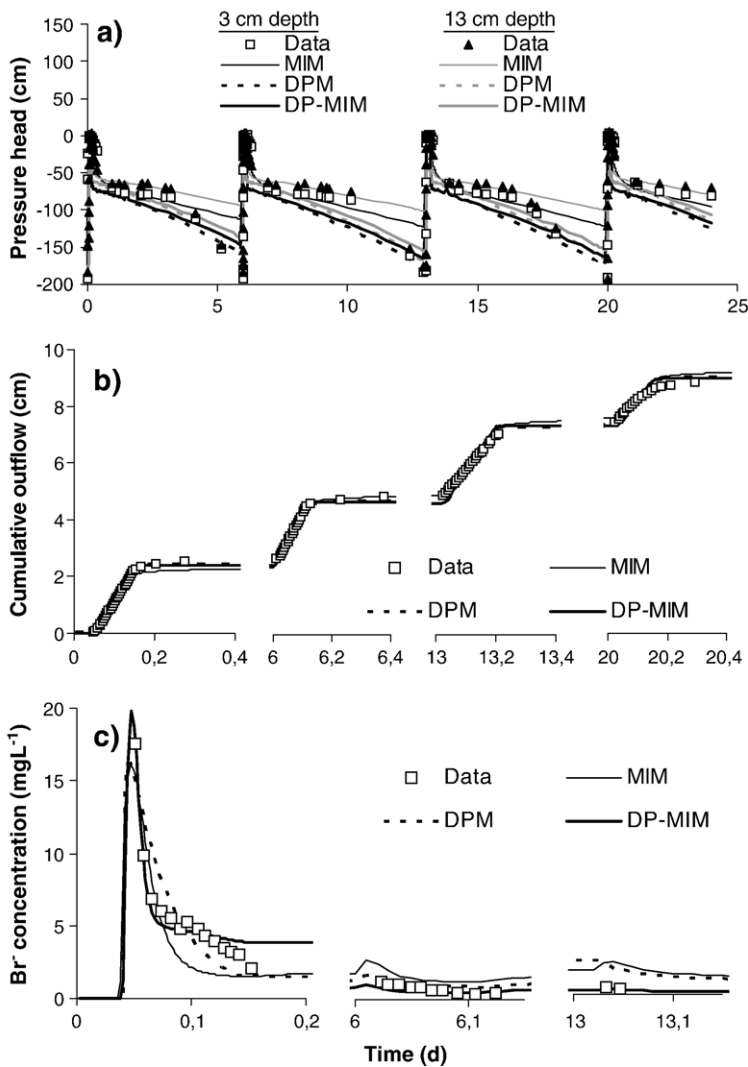


Fig. 3. Transient water flow and bromide (Br^-) transport data from the Ah-soil column, and corresponding model simulation results, a) pressure heads at depths of 3 and 13 cm, b) cumulative outflow, and c) Br^- effluent concentrations.

approach simulated the low measured Br^- concentrations during the second week (Fig. 3c). This visual evaluation was again supported by the E -statistics that increased from 0.449 for MIM to 0.644 for DPM and 0.818 for DPM–MIM, with MAE decreasing in the same order (Table 4).

The narrow Br^- BTC in the Ah soil was reflected by a ω_h value 10 times smaller than for the Ap soil (Table 4). In the MIM, the $K_{s,mo}$ was larger for Ah than for the Ap soil, as expected for the more pronounced preferential flow. However, for the DPM and DP-MIM, values for $w_f K_{s,f}$ were smaller for Ah than for Ap, and this discrepancy remained even for local $K_{s,f}$ values obtained by dividing $w_f K_{s,f}$ (Table 4) by w_f . However, the $K_{s,f}$ values for the Ap soil were overestimated as explained above. Moreover, smaller α_f and larger n_f values for Ah (Table 4) mean relatively larger unsaturated K_f values than for Ap. Hence, $K_{s,f}$ values fitted under variably saturated conditions

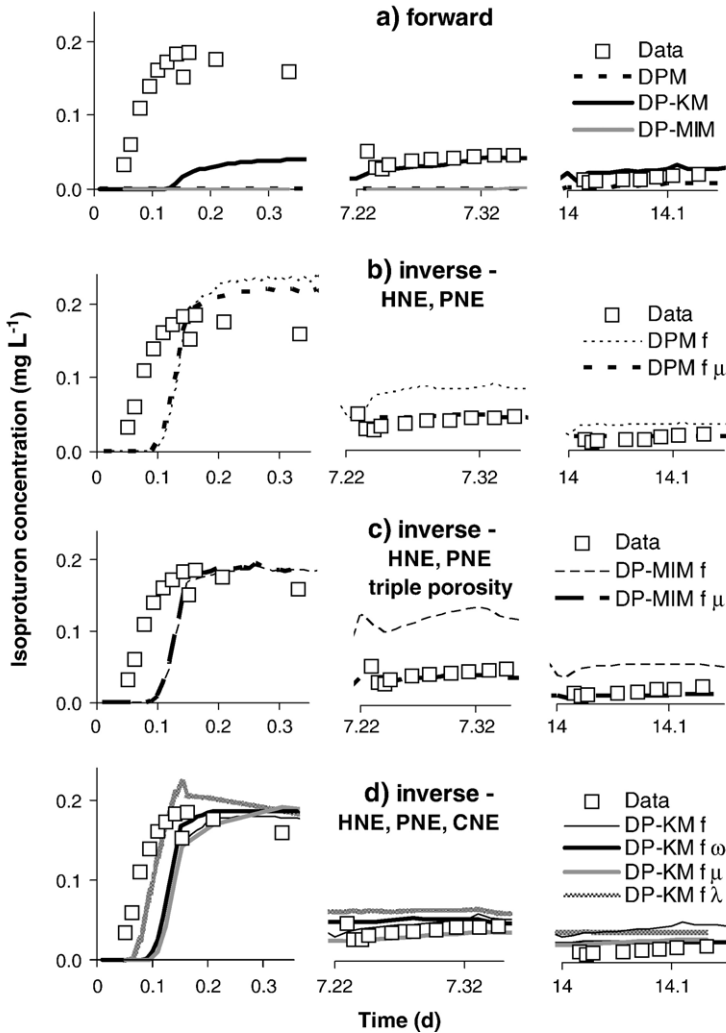


Fig. 4. Transient water flow and isotopuron (IPU) transport data from the Ap-soil column, and corresponding model simulation results, a) forward simulations, b) inverse simulation 1, c) inverse simulation 2, and d) inverse simulation 3 (DPM $f\mu$ indicates the dual permeability model with fitted f and μ parameters).

are less suitable indicators of the extent of preferential flow than, e.g., ω_h and ω_p . As expected, the ω_p values in MIM and DPM were also smaller for Ah than for Ap. Only for the DP-MIM approach, ω_p^{DPM} (3.62 d^{-1}), ω_p^{MIM} (0.07 d^{-1}) and θ_{im} (0.222) were larger, and λ_f (0.42 cm) smaller than for Ap (Table 4). We note that for all approaches, ω_p and λ_f were to some extent negatively correlated ($-0.7 < r^2 < -0.3$, not further shown). The best fit of the Br^- BTC suggests that the DP-MIM triple-porosity approach best represented the dispersivity and solute transfer between macropores, inter-aggregate regions, and aggregates of the Ah soil. The small λ_f (0.42 cm) value estimated using DP-MIM may consequently best represent the actual dispersivity of the macropore domain of the Ah soil column. The striking differences between ω_f and ω_p values for the relatively similar model approaches (Table 4) point to the need of further improving experimental designs for parameter identification of two- and multi-region models.

Overall, the two-region concept appeared to be a reasonable approximation of the actual HNE and PNE solute transport in the Ah soil, with the two mobile regions of the DPM approach providing a somewhat better description of the data. The decrease of Br^- concentrations at later times, similarly as for the Ap soil, could be reproduced only with the DP-MIM approach that considered diffusive solute transfer into an immobile sub-region of the matrix.

3.3. Herbicide transport

3.3.1. Ap soil column: isoproturon transport

For the weakly adsorbed herbicide IPU, Fig. 4 shows the measured BTC together with simulation results using various forward (Fig. 4a) and inverse (Fig. 4b,c,d) modeling approaches. Isoproturon appeared simultaneously with Br^- in the effluent, but at much lower peak

Table 5

Isoproturon transport parameters and corresponding (\pm) 95% confidence limits for the various model approaches used for simulating the observed IPU breakthrough curve in the **Ap soil column**

Approach	$f_{\text{mo}}, f_{\text{f}}^{\S}$	$\omega_{\text{c},\text{f}}$ (d^{-1})	$f_{\text{m}}, f_{\text{mo}}^{\dagger}$	$\lambda_{\text{mo}}, \lambda_{\text{f}}^{\ddagger}$ (cm)	μ (d^{-1})	E (MAE) (mg L^{-1})
<i>Forward</i>						
MIM	0.408	–	–	2.30	0.046	–0.54 (0.088)
DPM	1	–	–	2.75	0.046	–0.54 (0.088)
DP-MIM	1	–	0.043	2.82	0.046	–0.25 (0.068)
DP-KM	0.375	0.105	0.375	2.75	0.046	0.03 (0.053)
<i>Inverse</i>						
DPM f	0.240 \pm 10.5	–	–	2.75	0.046	0.30 (0.038)
DPM $f\mu$	0.240 \pm 0.001	–	–	2.75	0.410 \pm 0.126	0.51 (0.026)
DP-MIM f	0.236 \pm 1.5	–	0.043	2.82	0.046	–0.01 (0.055)
DP-MIM $f\mu$	0.229 \pm 0.005	–	0.043	2.82	0.761 \pm 0.146	0.49 (0.028)
DP-KM f	0.258 \pm 2.8	0.105	0.375	2.75	0.046	0.40 (0.033)
DP-KM $f\omega$	0.242 \pm 0.003	0.045 \pm 0.024	0.375	2.75	0.046	0.48 (0.028)
DP-KM $f\mu$	0.254 \pm 0.001	0.105	0.375	2.75	0.421 \pm 0.221	0.45 (0.030)

Fitted parameters are in bold letters. Default parameters see in Tables 3 and 4; ω_p^{MIM} and ω_p^{DPM} (Table 4) were multiplied by diffusion correction factor 0.39 (=0.7/1.797). \S Fraction of sorption sites in the mobile region (f_{mo} ; MIM), or factor to increase or decrease sorption in the fracture pore system (f_{f} ; DPM, DP-MIM), or fraction of equilibrium sorption sites in the fracture pore system (f_{f} ; DP-KM). Multiply f_{f} with w_{f} (0.2) to obtain global value ($f_{\text{f}} w_{\text{f}}$) that can be compared with f_{mo} . \dagger Fraction of equilibrium sorption sites in the matrix (f_{m} ; DP-KM) or fraction of sorption sites in the mobile region of the matrix (f_{mo} ; DP-MIM). \ddagger Dispersivity in the mobile region (λ_{mo} ; MIM) or in the fracture pore system (λ_{f} ; DPM, DP-MIM, DP-KM).

concentrations below 0.2 mg L^{-1} . The IPU breakthrough was characterized by concentration drops during redistribution times between irrigations, which were not observed in Br^- breakthrough.

The MIM forward approach predicted zero concentrations for all times (not shown), and the MIM was not further evaluated for inverse parameter estimation. While none of the forward modeling approaches approximated the observed IPU breakthrough, only DP-KM predicted an early concentration increase (Fig. 4). Accordingly, among the forward approaches only DP-KM had a non-negative E statistics (Table 5). Hence, DP-KM forward simulation results confirm the relevance of kinetic sorption (CNE) for IPU transport.

However, the DPM and DP-MIM equilibrium sorption approaches apparently much improved when fitting only f_f (Fig. 4b,c), even if huge confidence intervals revealed large uncertainty for fitting f_f alone (Table 5). Note that we refer to DPM with optimized parameter f_f as DPM f in Fig. 4b and that we use similar notation for other inverse optimizations. Inverse estimates were similar for the DPM f ($f_f=0.240$) and DP-MIM f ($f_f=0.236$), and were thus four times smaller than assumed in the forward simulations (Table 5). The IPU concentrations after

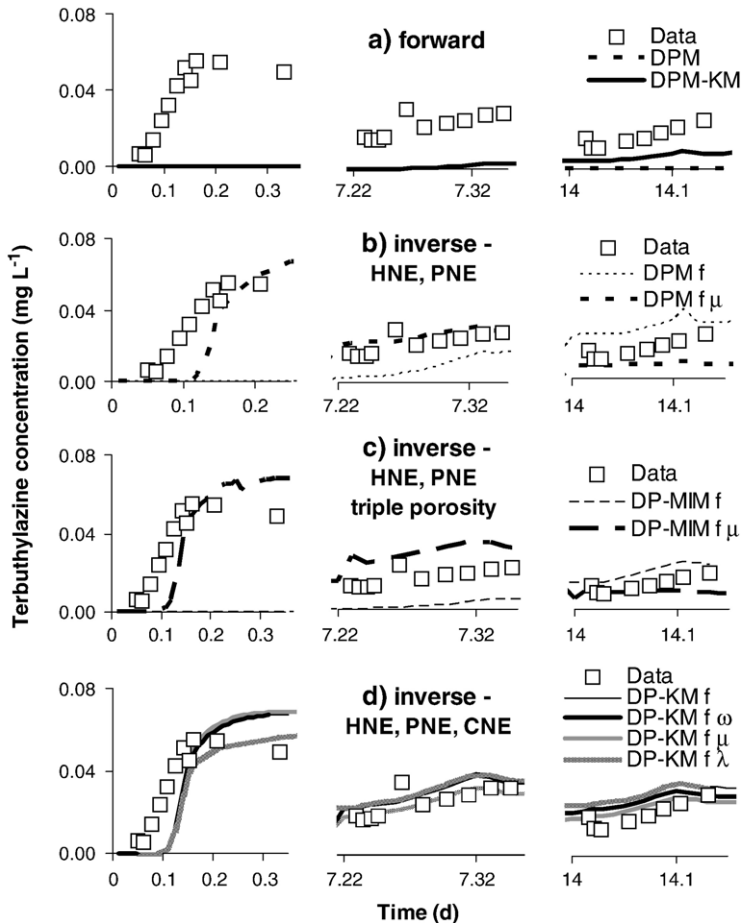


Fig. 5. Transient water flow and terbuthylazine (TER) transport data from the Ap-soil column, and corresponding model simulation results, a) forward simulations, b) inverse simulation 1, c) inverse simulation 2, and d) inverse simulation 3.

one week were overestimated with DPM (Fig. 4b) and even more so with DP-MIM (Fig. 4c), which resulted in acceptable ($E=0.301$) and poor ($E=-0.011$) model performance for DPM and DP-MIM, respectively. When f_f and μ were both fitted in DPM and DP-MIM, the IPU concentrations after one week were matched well (Fig. 4b,c), which increased E to values around 0.5 (Table 5). Estimates for f_f hardly changed (with associated confidence intervals drastically decreased), while μ increased from 0.046 to 0.41 d⁻¹ (DPM $f\mu$) or 0.76 d⁻¹ (DP-MIM $f\mu$) corresponding to very short half-lives of only 1.7 or 0.9 days for DPM $f\mu$ and DP-MIM $f\mu$, respectively.

The best BTC match ($E=0.40$; Table 5) when fitting only f_f ($=0.258$) was achieved using the inverse DP-KM f (Fig. 4d). Gradual further improvement for late times was obtained by fitting f_f and $\omega_{c,f}$ ($E=0.48$), or f_f and μ ($E=0.45$), giving very similar curves (Fig. 4d, Table 5). The observed IPU loss of 0.090 mg or 7.1% of 1.27 mg IPU applied was approximated by the model approaches, e.g., the DP-KM $f\omega$ approach simulated a mass loss of 0.074 mg or 5.8%. Additionally, the hypothesis was tested that λ_f may be different for conservative Br⁻ and nonlinearly adsorbed IPU. Jointly optimizing λ_f with f_f resulted in the best approximation of the first IPU peak (Fig. 4d). However, the large positive correlation ($r>0.9$) between λ_f (15 cm; at upper constraint) and f_f showed that these two parameters could not be identified simultaneously.

3.3.2. Ap soil column: terbuthylazine transport

The measured and simulated TER BTCs are shown in Fig. 5 for forward (Fig. 5a) and inverse (Fig. 5b,c,d) approaches. The breakthrough of the more strongly adsorbed TER started simultaneously with Br⁻ and IPU, but at still lower concentrations below 0.06 mg L⁻¹. Forward

Table 6

Terbuthylazine (TER) transport parameters and corresponding (\pm) 95% confidence limits for various model approaches used for simulating the observed TER breakthrough curve in the **Ap soil column**

Approach	f_{mo}, f_f^{\S}	$\omega_{c,f}$ (d ⁻¹)	f_{mo}, f_{mo}^{\dagger}	$\lambda_{mo}, \lambda_f^{\ddagger}$ (cm)	μ (d ⁻¹)	E (MAE) (mg L ⁻¹)
<i>Forward</i>						
MIM	0.408	–	–	2.30	0.011	-1.36 (0.026)
DPM	1	–	–	2.75	0.011	-1.36 (0.026)
DP-MIM	1	–	0.043	2.82	0.011	-1.36 (0.026)
DP-KM	0.499	0.106	0.499	2.75	0.011	-1.18 (0.024)
<i>Inverse</i>						
DPM f	0.401 \pm 1.6	–	–	2.75	0.011	-0.93 (0.021)
DPM $f\mu$	0.191 \pm 0.002	–	–	2.75	1.0 [¶] \pm 0.070	0.01 (0.012)
DP-MIM f	0.500 \pm 1.6	–	0.043	2.82	0.011	-1.04 (0.022)
DP-MIM $f\mu$	0.185 \pm 0.003	–	0.043	2.82	1.0 [¶] \pm 0.052	-0.19 (0.012)
DP-KM f	0.188 \pm 3.4	0.106	0.499	2.75	0.011	0.21 (0.008)
DP-KM $f\omega$	0.189 \pm 0.003	0.095 \pm 0.037	0.499	2.75	0.011	0.20 (0.008)
DP-KM $f\mu$	0.186 \pm 0.002	0.106	0.499	2.75	0.340 \pm 0.113	0.37 (0.006)

Fitted parameters are in bold letters. See Tables 3 and 4 for default parameters. [§]Fraction of sorption sites in the mobile region (f_{mo} ; MIM), or factor to increase or decrease sorption in the fracture pore system (f_f ; DPM, DP-MIM), or fraction of equilibrium sorption sites in the fracture pore system (f_f ; DP-KM). Multiply f_f with w_f (0.2) to obtain global value ($f_f w_f$) that can be compared with f_{mo} . [†]Fraction of equilibrium sorption sites in the matrix (f_{mo} ; DP-KM) or fraction of sorption sites in the mobile region of the matrix (f_{mo} ; DP-MIM). [¶]Dispersivity in the mobile region (λ_{mo} ; MIM) or in the fracture pore system (λ_f ; DPM, DP-MIM, DP-KM).

simulations did not match observed concentrations, with only DP-KM predicting concentrations gradually increasing after one week (Fig. 5a).

The inverse DPM (DP-MIM) approaches failed to simulate TER breakthrough when fitting f_{mo} (f_f) alone, but simulations improved upon concurrent inverse estimation of f_{mo} and μ (f_f and μ) (Fig. 5b,c). However, based on zero or negative E , neither approach reproduced TER breakthrough any better than the mean TER concentration (Table 6).

Significant further improvement could only be attained using the DP-KM approach (Fig. 5d). According to the E statistics, acceptable simulation results were achieved by inverse estimation of f_f (0.188) yielding $E=0.21$, while simultaneously fitting f_f and μ further increased E to 0.37 (Table 6). Simultaneous estimation with f_f made μ reach its upper constraint of 1.0 d^{-1} in DPM and DP-MIM, while μ reached 0.34 d^{-1} in the DP-KM $f_f\mu$ approach (Table 6). Simultaneously fitting λ_f and f_f in DP-KM did not significantly improve the simulation results (Fig. 5d).

Mean absolute deviations, MAE, were smaller for TER than for IPU, due to smaller TER concentrations. The estimation of the total TER mass loss after 14.2 days using the DP-KM $f_f\mu$ approach was quite accurate. While the observed mass loss was 0.039 mg or 2.3% of the applied 1.45 mg TER, the simulated loss was 0.031 mg or 2.1%.

3.3.3. Ah soil column: isotoproturon transport

Results for the IPU breakthrough are illustrated in Fig. 6 along with corresponding forward (Fig. 6a) and inverse (Fig. 6b) model simulations. The IPU BTC displayed the same extremely left-skewed shape as Br^- , peaking already in the first column effluent, which is characteristic of preferential flow. The peak concentration of 3 mg L^{-1} was over 10 times higher than the IPU peak in the Ap soil column. Furthermore, the IPU BTC did not show concentration drops during redistribution phases (Fig. 6), in contrast to herbicide BTCs in the Ap soil column (Figs. 4, 5).

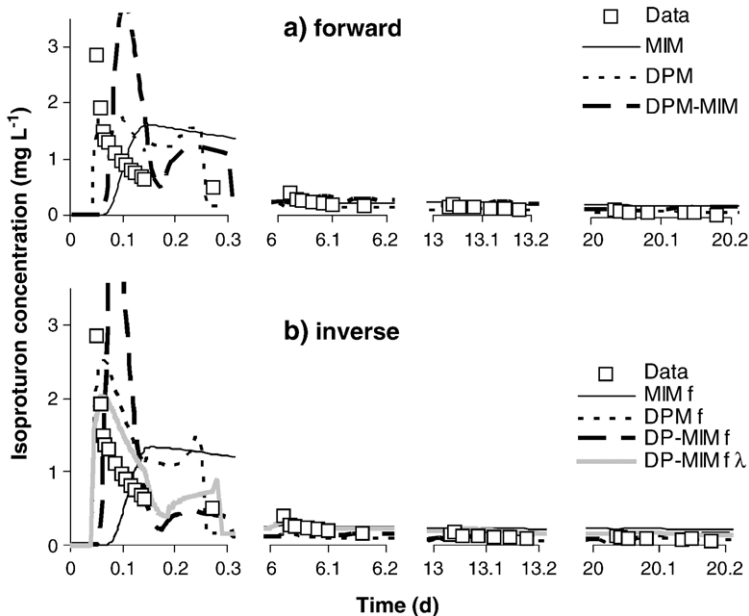


Fig. 6. Isoproturon (IPU) transport data from the Ah-soil column, and corresponding model simulation results, a) forward simulations, b) inverse simulation.

Table 7

Isoproturon (IPU) and Terbutylazine (TER) transport parameters and corresponding (\pm) confidence limits for various model approaches used for simulating the observed IPU breakthrough curve in the Ah soil column

Approach	Isoproturon				Terbutylazine				
	f_f, f_{mo}^{\S}	f_m, f_{mo}^{\dagger}	$\lambda_{mo}, \lambda_f^{\ddagger}$ (cm)	E (MAE) (mg L ⁻¹)	f_f, f_{mo}^{\S}	f_m, f_{mo}^{\dagger}	$\lambda_{mo}, \lambda_f^{\ddagger}$ (cm)	E (MAE) (mg L ⁻¹)	
<i>Forward</i>									
MIM	0.150	0.850	2.34	0.12(0.41)	0.150	0.850	2.34	-0.39(0.19)	
DPM	1	-	10.0	0.15(0.39)	1	-	10.0	-0.09(0.15)	
DP-MIM	1	0.363	0.42	-0.34(0.61)	1	0.363	0.42	-0.12(0.16)	
<i>Inverse</i>									
MIM f	0.174 \pm 1.2	0.826	2.34	0.17 (0.38)	0.084 \pm 12.6	0.916	2.34	0.01 (0.14)	
DPM f	0.728 \pm 17.2	-	10.0	0.36 (0.29)	1.260 \pm 3.3	-	10.0	0.34(0.09)	
DP-MIM f	0.705 \pm 13.1	0.363	0.42	-0.21 (0.55)	0.855 \pm 100	0.363	0.42	-0.30(0.18)	
DP-MIM $f\lambda$	1.548 \pm 0.04	0.363	15 [#]	0.54 (0.21)	1.825 \pm 0.09	0.363	15 [#]	0.44(0.08)	

Fitted parameters are in bold letters. Fixed: β (IPU)=0.89, μ (IPU)=0.046 d⁻¹, β (TER)=0.92, μ (TER)=0.011 d⁻¹, and parameters in Tables 3 and 4. [§]Fraction of sorption sites in contact with the mobile region (f_{mo} – MIM) or empirical factor to increase or decrease sorption in the fracture pore system (f_f ; DPM, DP-MIM). Multiply f_f with w_f (0.05) to obtain global value ($f_f w_f$) that can be compared with f_{mo} . [†]Fraction of equilibrium sorption sites in the matrix (f_m ; DP-KM) or fraction of sorption sites in contact with mobile region within the matrix (f_{mo} ; DP-MIM). [‡]Dispersivity the mobile region (λ_{mo} ; MIM) or in the fracture pore system (λ_f ; DPM, DP-MIM). [#]At upper constraint.

The MIM, DPM and DP-MIM forward approaches assuming instantaneous sorption provided much better predictions of the observed IPU BTC for the Ah (Fig. 6a) than corresponding forward models did for the Ap soil column. Furthermore, the DP-KM approach did not yield further improvement, even when optimizing f_f and $\omega_{c,f}$ (not shown). These results suggest that there was sorption equilibrium within the PFP of the Ah soil column even during fast preferential transport.

Both DPM and DP-MIM predicted secondary peaks around 0.25 days. However, around 0.25 days the column outflow almost ceased (Fig. 3b), such that only one sample could be retrieved between 0.15 and 0.3 days (Fig. 6). Due to minimal outflow, the relevance of the secondary peaks for simulated IPU mass loss was negligible.

The best (acceptable) goodness-of-fit statistics among the forward approaches (Table 7) was obtained for the DPM ($E=0.15$). Optimizing f_f improved the DPM description of the IPU BTC (Fig. 6b) and provided the best goodness-of-fit ($E=0.36$). The total IPU mass loss after 20.2 days (0.54 mg or 32% of applied) was somewhat overestimated using the DPM f approach (0.81 mg or 48%). The inverse DP-MIM f and MIM f simulations could not approximate the first IPU peak (Fig. 6b, Table 7). For DPM f and DP-MIM f approaches, inverse estimates for f_f were slightly above 0.7 (Table 7). Estimating both f_f and μ gave no overall improvement for any approach (not shown), while fitted large values of f_f and λ (Table 7) at moderate correlation ($r=0.4$) enabled the DP-MIM to simulate the early IPU BTC rise (Fig. 6b).

3.3.4. Ah soil column: terbutylazine transport

Finally, breakthrough data and simulation results for the more strongly adsorbed herbicide TER are depicted in Fig. 7 for forward (Fig. 7a) and inverse (Fig. 7b) model approaches. The TER BTC appeared concurrently as IPU and Br⁻, but with a less sharp and lower peak of 0.5 mg L⁻¹. The agreement between models and observed TER concentrations was less good than for IPU (Fig. 7). The forward MIM approach severely underestimated TER concentrations.

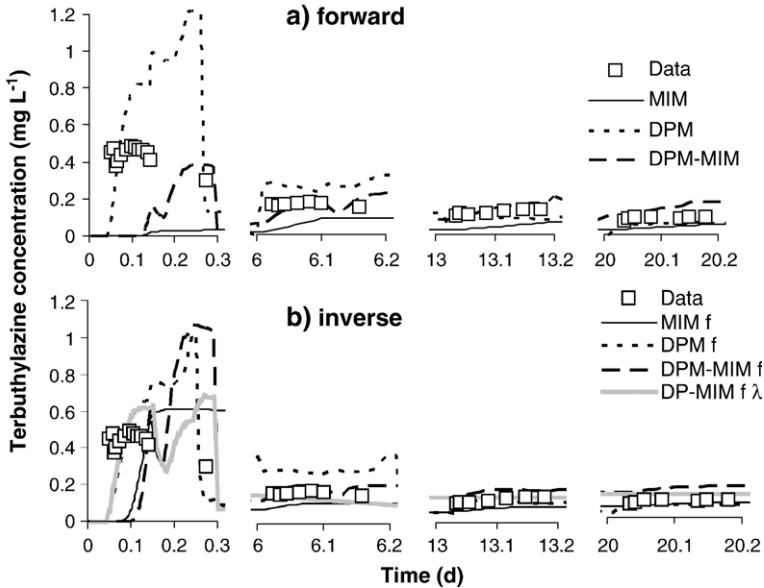


Fig. 7. Terbutylazine (TER) transport data from the Ah-soil column, and corresponding model simulation results, a) forward simulations, b) inverse simulation.

The forward DPM approach predicted the early TER appearance in the effluent, but overestimated the peak concentration. The DP-MIM approach predicted a later TER concentration increase than observed (Fig. 7a).

Inverse estimation of f_{mo} improved the agreement between MIM results and data, but without a prediction of the early increase of TER concentrations. Among all approaches, fitting f_f in the DPM approach resulted in the best (acceptable) agreement with the data ($E=0.338$, $\text{MAE}=0.09 \text{ mg L}^{-1}$, Table 7). The total TER mass loss after 20.2 days was reproduced using the DPM f approach. While the observed mass loss was 0.31 mg or 20% of the applied 1.57 mg IPU, the simulated mass loss was 0.33 mg or 21%. In DP-MIM, the early peak could not be reproduced by fitting f_b , even when assigning higher weights, $w_{i,j}$, to initial TER observations (Table 7, approach DPM-MIM f).

For DPM f and DP-MIM f approaches, inverse estimates for f_f were above and below one, respectively (Table 7). Again, joint optimization of f_f and μ did not improve results (not shown), while fitted large values of f_f and λ (Table 7) in the DP-MIM improved simulation of the early TER BTC rise (Fig. 7b).

4. Discussion

4.1. Sorption

For the Ap soil column, the inverse DPM, DP-MIM, and DP-KM simulations of IPU transport produced comparable estimates for f_f (0.19 to 0.27). Slightly smaller f_f values (0.16 and 0.19) were found for the more strongly adsorbed TER. Overall, DPM and DP-MIM inverse simulation results suggest small equilibrium sorption capacity in the PFPs, while the DP-KM approach suggests rate-limited sorption in the PFPs. There is however much evidence for the

latter explanation: (i) IPU and TER batch tests revealed kinetic sorption in the bulk soil, (ii) among forward simulations only the DP-KM predicted fast herbicide leaching, (iii) among model approaches with only f_f fitted, the DP-KM best described the herbicide concentration drops during the one-week redistribution period.

For the Ah soil column, where herbicide sorption was instantaneous according to batch test results, the inverse herbicide transport simulations yielded larger f_f values of around one (or above one, if λ_f was additionally fitted). The f_f values above one were in accord with reported findings of batch tests that organic linings of earthworm burrows may increase the sorption as compared to the soil matrix (Stehouwer et al., 1993, 1994; Mallawatantri et al., 1996). On the other hand, the predictive capacity of batch sorption tests performed with material scratched from earthworm burrows may be limited for transport conditions with variable saturation, where effects such as partial wetting of burrow walls might counterbalance the increased sorption.

Sorption often appeared to be reduced in mobile soil water regions of aggregated or structured soils, as we found for our Ap soil column. For example, Vanderborght et al. (2002) utilized MIM simulations of Cl^- and fluorescent dye tracer transport in undisturbed soil columns at steady-state flow and found a smaller sorption capacity of the mobile region, f_{mo} , for the more strongly adsorbed dye sulforhodamine B ($f_{\text{mo}} < \theta_{\text{mo}}/\theta$) than for brilliant sulfaflavine ($f_{\text{mo}} = \theta_{\text{mo}}/\theta$). This finding was experimentally confirmed by measurements of lower sulforhodamine B concentrations in the mobile region (Vanderborght et al., 2002). Applications of the dual-permeability model MACRO for simulating preferential pesticide leaching yielded values for the fraction of sorption sites in the macropore, f , which appear rather small (although direct comparison with f_{mo} or $w_f f_f$ values is limited by the conceptual model differences). For example, f in MACRO was assumed to be 0.02 to describe bentazone leaching (Larsson and Jarvis, 1999) and f was fitted to values ranging from 0.008 to 0.048 to describe transport of the herbicide MCPA in different soils (Roulier and Jarvis, 2003a). The latter authors found f to be associated with large estimation uncertainty (Roulier and Jarvis, 2003a,b), which is in agreement with our results showing large confidence intervals for f_f when fitted alone.

In our inverse DPM and DP-MIM simulations of herbicide transport in the Ap soil column, the strong reduction of f_f (from unity down to 0.2) as compared to less reduction of f_f (from batch test values) in the DP-KM approach suggest that some previously reported small f estimates may simply result from ignoring chemical nonequilibrium. The acceleration of pesticide leaching by slow sorption reaction rates within the preferential flow domain was also shown by comparing dual-permeability model scenarios with kinetic and equilibrium sorption (Ray et al., 2004).

In a recent study by Pot et al. (2005), a set of experiments to study the transport of Br^- , IPU, and metribuzin through structured undisturbed soil columns was performed at five different steady-state flow rates. The effect of flow velocity on herbicide transport was evaluated using comparable models as in our study. Herbicide sorption in the preferential flow region was found to be kinetic, and only combined PNE–CNE models were successful in simulating the BTCs. Similar as for our Ap soil, no model could capture the early rise of the herbicide concentrations, while the DP-KM approach yielded the best agreement with the observed BTCs. The DP-KM approach for low and intermediate flow velocities gave similar values ($f_f = 0.22$ to 0.29) as for our Ap column, while f_f was lower for the highest flow velocity ($f_f = 0.12$).

4.2. Degradation

For IPU and TER leaching in the Ap soil column, inverse estimation gave values for the first-order degradation rate in the liquid phase, μ , in the range of 0.3 – 1.0 d^{-1} , while typical values

are at least an order of magnitude smaller (e.g., James et al., 1998; Walker et al., 2002). Much larger magnitudes of degradation rates in laboratory column studies (particularly under unsaturated flow conditions) as compared to batch sorption experiments were found before, and the results of several such studies were reviewed in Pot et al. (2005). For example for inverse simulation of MCPA transport using the MACRO model, μ values of 0.3–0.4 d⁻¹ were apparently well identified with very low uncertainty (Roulier and Jarvis, 2003a). In transport experiments under unsaturated flow conditions, Pot et al. (2005) found μ values up to 31 (IPU) and 18 times (metribuzin) larger than the literature values (Agritox, 2001). However, the degradation constant increased with the extent of nonequilibrium sorption, such that the estimated high degradation rates may have only reflected chemical irreversible or hysteretic sorption, defined as fast attachment and much slower detachment. Irreversible or hysteretic sorption may thus have been lumped together with degradation and mineralization into μ (Pot et al., 2005). This argument can be corroborated to some extent by our own results. While fitting of μ did not improve simulation results for the Ah soil where kinetic (irreversible) sorption was not involved, it did apparently improve simulations of herbicide transport in the Ap soil where kinetic sorption was important. Moreover, jointly optimizing f_f and $\omega_{c,f}$ or f_f and μ in DP-KM (and even f_f and μ in DPM and DP-MIM) produced comparable simulated BTCs. Hence, effects of sorption rate, $\omega_{c,f}$, and degradation rate, μ , on herbicide transport cannot be jointly identified based on BTC fitting.

4.3. Dispersion

For the Ah soil, DP-MIM was the best approach for simulating Br⁻ transport but not for simulating herbicide transport. This discrepancy could be explained when assuming that the dispersivity was not the same for Br⁻ and herbicides. For example, Vanderborght et al. (2002) found that MIM simulation results of dye tracer BTCs could be significantly improved when assuming different dispersivity values for two different dyes. Recently, a number of studies reported increased dispersivity of adsorbed as compared to conservative chemicals (e.g., Pot and Genty, 2005), this increase being more pronounced for nonlinearly than linearly adsorbed chemicals (e.g., Vanderborght et al., in press). The same relations should be evaluated for the dispersivity within pore regions of two-flow region models. As a first indication, the description of IPU and TER breakthrough through the Ap and Ah soil columns improved when λ_f was optimized to larger values than were obtained for Br⁻ breakthrough.

4.4. Limitations of the approach

Despite the advanced models and the comprehensive data used in this study, there are some limitations to our approach. To overcome these limitations will require further experimental and model refinement. For example even for conservative solute transport, two-region model parameters may depend on time and length scales, as well as boundary conditions used in the experiment (Young and Ball, 2000). For reactive nonequilibrium solute transport, the parameters f_f , ω_c , and μ seemed to depend on flow rate, water saturation, and degree of nonequilibrium (Pot et al., 2005). Although the transient flow conditions with wetting and drying cycles used in this study approximate better the natural flow conditions, fitted parameters may only reflect effective values averaged over variable saturations and flow velocities. Little is known about how natural transient flow conditions affect average parameters. Improved experimental techniques are required to separate real functional dependences of model parameters on flow

conditions from model artefacts. For examples, incorrect sorption parameter values can be obtained when equilibrium conditions are not fully understood (Sabbah et al., 2005), and analyzing solute breakthrough curves alone may not be sufficient to separate effects of degradation and irreversible sorption (Pot et al., 2005). For better parameter identification, column experiments will need to be augmented with data about local processes within the column. Examples would be flow path visualization and local concentration measurements using computer tomography and dye tracers (e.g., Vanderborght et al., 2002), or measurements of adsorbed herbicide concentrations in preferential flow paths and matrix at the end of the experiment. Furthermore, possibly inadequate first-order water and solute transfer terms may cause the dependence of optimized transport parameters on time and length scales. A second-order water transfer term was shown to give higher accuracy for the two-region model simulation of preferential water flow (e.g., Köhne et al., 2004). Similarly, the improved accuracy gained by using second-order (advective and) diffusive solute transfer terms on solute transport under (transient and) steady-state flow should be evaluated.

5. Conclusions

For the aggregated Ap soil column, the BTCs of Br^- , IPU, and TER started simultaneously suggesting preferential flow conditions. Peak concentrations decreased in the order of Br^- , IPU, and TER, due to increasing sorption in accordance with batch test results. The inverse DPM simulation of water flow and Br^- transport revealed HNE and PNE. Inverse DPM and DP-MIM simulations could apparently approximate the herbicide breakthrough curves when fitting reduced equilibrium sorption in the preferential flow paths. However, the DP-KM approach revealed that herbicide transport in the fracture pore region of the Ap soil column was governed by rate-limited sorption. Furthermore, large optimized degradation rates were estimated only for the Ap soil. However, comparable simulated BTCs were obtained when either the degradation or sorption rates were optimized. Our results therefore suggest that it may not be possible to inversely identify the degradation rate in nonequilibrium transport models from a BTC if transport is affected by time-dependent sorption.

The Ah soil column contained crumbs and an earthworm burrow. The BTCs of IPU and Br^- featured narrow early peaks characteristic of preferential flow, while the TER breakthrough displayed an early but less sharp initial peak. Inverse DPM simulations of water flow and Br^- displacement revealed HNE and PNE as for the Ap soil, while batch experiments revealed instantaneous sorption (no CNE) for IPU and TER in the Ah soil. This was confirmed by the model analysis of herbicide transport where assuming kinetic sorption did not improve the model-data agreement. The forward simulation using the DPM (equilibrium sorption) approach gave an acceptable approximation of the IPU BTC. This suggests that in the absence of CNE, more reliable predictions of preferential herbicide transport can be made based on standard batch sorption tests and hydraulic and tracer transport data, than in the presence of CNE. As expected from the observed triple-porosity structure (macropore, inter-aggregate region, aggregates) of the Ah soil column, the DP-MIM was the best approach for simulating the Br^- BTC, with transport after two weeks controlled by slow diffusion into the immobile part of the matrix. However, it was the DPM and not the DP-MIM that provided the best description of the IPU and TER breakthrough. No obvious reason was found for this discrepancy, other than the possibility that the dispersivity may be different for conservative and (nonlinearly) adsorbed solutes.

Overall, modeling our data permitted identification of different processes involved in herbicide transport through variably saturated structured soil. For the aggregated Ap soil column,

herbicide transport was under complex HNE–PNE–CNE conditions with rate-limited sorption, while herbicide transport through the macroporous Ah soil column during pronounced preferential flow was only under HNE–PNE conditions with equilibrium sorption, which shows that sorption kinetics in structured soils is not necessarily related to the extent of preferential flow. However, to describe the herbicide transport in structured soils requires many parameters for models of increasing complexity. To ensure realistic process description, as many model parameters as possible should be identified independently, and column experiments need to be further developed to facilitate parameter identification in complex multi-process flow-transport models.

Acknowledgements

We wish to thank Valérie Pot and an anonymous reviewer for helpful comments. The development of nonequilibrium flow and transport models was partly supported by the Terrestrial Sciences Program of the Army Research Office (Terrestrial Processes and Landscape Dynamics and Terrestrial System Modeling and Model Integration).

References

- Agritox, 2001. Toxicological Data Base on Pesticides. INRA, France.
- Atkins, P.W., 1990. Physical chemistry. 995 p., 4th ed. New York.
- Ball, W.P., Roberts, P.V., 1991. Long-term sorption of halogenated organic chemicals by aquifer materials: Part 2. Intraparticle diffusion. *Environ. Sci. Technol.* 25 (7), 1237–1249.
- Berglof, T., Koskinen, W.C., Duffy, M.J., Norberg, K.A., Kylin, H., 2003. Metsulfuron methyl sorption–desorption in field-moist soils. *J. Agric. Food Chem.* 51 (12), 3598–3603.
- Brusseau, M.L., Rao, P.S.C., 1989. The influence of sorbate-organic matter interactions on sorption nonequilibrium. *Chemosphere* 18, 1691–1706.
- Brusseau, M.L., Jessup, R.E., Rao, P.S.C., 1989. Modeling the transport of solutes influenced by multiprocess nonequilibrium. *Water Resour. Res.* 25, 1971–1988.
- Cameron, D.R., Klute, A., 1977. Convective-dispersive solute transport with a combined equilibrium and kinetic adsorption model. *Water Resour. Res.* 13, 183–187.
- Celis, R., Cox, L., Hermosin, M.C., Cornejo, J., 1997. Sorption of thiazafuron by iron- and humic acid-coated montmorillonite. *J. Environ. Qual.* 26, 472–479.
- Chen, S., Franklin, R.E., Johnson, A.D., 1997. Clay film effects on ion transport in soil. *Soil Sci.* 162 (2), 91–96.
- Cooke, C.M., Shaw, G., Collins, C.D., 2004. Determination of solid–liquid partition coefficients (K_d) for the herbicides isoproturon and trifluralin in five UK agricultural soils. *Environ. Pollut.* 132 (3), 541–552.
- Czapar, G.F., Horton, R., Fawcett, R.S., 1992. Herbicide and tracer movement in soil columns containing an artificial macropore. *J. Environ. Qual.* 21, 110–115.
- Dubus, I.G., Brown, C.D., 2002. Sensitivity and first-step uncertainty analysis for preferential flow model MACRO. *J. Environ.* 31, 227–240.
- Flury, M., 1996. Experimental evidence of transport of pesticides through field soils—a review. *J. Environ. Qual.* 25, 25–45.
- Gamerding, A.P., Wagenet, R.J., van Genuchten, M.T., 1990. Application of two-site/two-region models for studying simultaneous nonequilibrium transport and degradation of pesticides. *Soil Sci. Soc. Am. J.* 54, 957–963.
- Gerke, H.H., Köhne, J.M., 2002. Hydraulic properties of soil aggregate skins. *Soil Sci. Soc. Am. J.* 66, 26–36.
- Gerke, H.H., van Genuchten, M.T., 1993. A dual-porosity model for simulating the preferential movement of water and solutes in structured porous media. *Water Resour. Res.* 29, 305–319.
- IVA-Industrieverband Agrar e.V., 1990. Wirkstoffe in Pflanzenschutz und Schädlingsbekämpfungsmitteln- Physikalische, chemische und toxikologische Daten: 2. Aufl. BLV Verlags-Gesellschaft, München.
- James, R.V., Rubin, J., 1979. Applicability of the local equilibrium assumption to transport through soil of solutes affected by ion exchange. In: Jenne, E.A. (Ed.), *Chemical Modeling of Aqueous Systems*. American Chemical Society, Washington, D.C., pp. 225–235.

- James, T.K., Rahman, A., Holland, P.T., McNaughton, D.E., Heiermann, M., 1998. Degradation and movement of terbuthylazine in soil. Proc. 51st N.Z. Plant Protection Conf., pp. 157–161.
- Jarvis, N., 1994. The MACRO model (version 3.1)-Technical description and sample simulations. Rep. and Diss., vol. 19. Dept. Soil Sci., Swed. Univ. of Agric. Sci., Uppsala, Sweden 51 pp.
- Kladivko, E.J., Brown, L.C., Baker, J.L., 2001. Pesticide transport to subsurface tile drains in humid regions of North America. *Crit. Rev. Environ. Sci. Technol.* 31 (1), 1–62.
- Köhne, J.M., 1999. Analyse präferentiellen Wasserflusses und Stofftransports in strukturierten Böden mit Hilfe eines Dual-Porositätsmodells. Doctoral thesis (in German, with English summary). In: Roweck, H., Lennartz, B. (Ed.), *Schriftenreihe Inst. Water Management and Landscape Ecology* 30, 173 pp. Christian-Albrechts-University, Kiel, Germany.
- Köhne, J.M., Mohanty, B.P., 2005. Water flow processes in a soil column with a cylindrical macropore: experiment and hierarchical modeling. *Water Resour. Res.* 41, W03010.
- Köhne, J.M., Gerke, H.H., Köhne, S., 200a. Effective diffusion coefficients of soil aggregates with surface skins. *Soil Sci. Soc. Am. J.* 66 (5), 1430–1438.
- Köhne, J.M., Köhne, S., Gerke, H.H., 2002b. Estimating the hydraulic functions of dual-permeability models from bulk soil data. *Water Resour. Res.* 38 (7).
- Köhne, J.M., Mohanty, B.P., Simůnek, J., Gerke, H.H., 2004. Evaluation of a second-order water transfer term for variably saturated dual-permeability flow models. *Water Resour. Res.* 40, W07409.
- Larsson, M., Jarvis, N., 1999. Evaluation of a dual-porosity model to predict field-scale solute transport in a macroporous soil. *J. Hydrol.* 215, 153–171.
- Legates, D.R., McCabe Jr., G.J., 1999. Evaluating the use of “goodness-of-fit” measures in hydrologic and hydroclimatic model validation. *Water Resour. Res.* 35 (1), 233–241.
- Ma, L., Selim, H.M., 1995. Transport of a nonreactive solute in soils: a two-flow domain approach. *Soil Sci.* 159 (4), 224–234.
- Ma, L., Selim, H.M., 1998. Physical nonequilibrium in soils: modeling and application. In: Selim, H.M., Ma, L. (Eds.), *Physical Nonequilibrium in Soils*. Ann Arbor Press, Chelsea, Michigan, pp. 83–115.
- Mallawatantri, A.P., McConkey, G.B., Mulla, M.J., 1996. Characterization of pesticide sorption and degradation in macropore linings and soil horizons of Thatuna silt loam. *J. Environ. Qual.* 25, 227–235.
- Meyer-Windel, S., 1998. Transport processes of bromide and herbicides under steady-state and transient flow conditions. PhD-dissertation, *Schriftenreihe Institut für Wasserwirtschaft und Landschaftsökologie der Christian-Albrechts-Universität zu Kiel*, 28, 113 pp.
- Meyer-Windel, S., Lennartz, B., Widmoser, P., 1999. Bromide and herbicide transport under steady-state and transient flow conditions. *J. Eur. Soil Sci.* 50, 23–33.
- Mualem, Y., 1976. A new model for predicting the hydraulic conductivity of unsaturated soils. Research Project Report, vol. 442. Technion, Israel Institute of technology, Haifa.
- Parrish, R.S., Smith, Ch.N., Fong, F.K., 1992. Tests of the pesticide root zone model and the aggregate model for transport and transformation of aldicarb, metolachlor, and bromide. *J. Environ. Qual.* 21, 685–697.
- Pennell, K.D., Hornsby, A.G., Jessup, R.E., Rao, P.S.C., 1990. Evaluation of five simulation models for predicting aldicarb and bromide behavior under field conditions. *Water Resour. Res.* 26 (11), 2679–2693.
- PerrinGanier, C., Breuzin, C., Portal, J.M., Schiavon, M., 1996. Availability and persistence of isoproturon under field and laboratory conditions. *Ecotoxicol. Environ. Saf.* 35 (3), 226–230.
- Pot, V., Simůnek, J., Benoit, P., Coquet, Y., Yra, A., Matrinez Cordün, M.-J., 2005. Impact of rainfall intensity on the transport of two herbicides in undisturbed grassed filter strip soil cores. *J. Contam. Hydrol.* 81 (1–4), 63–88.
- Pot, V., Genty, A., 2005. Sorbing and non-sorbing solute migration in rough fractures with a multi-species LGA model: dispersion dependence on retardation and roughness. *Transp. Porous Media* 59, 175–196.
- Rambow, J., Lennartz, B., 1993. Laboratory method for studying pesticide dissipation in the vadoze zone. *Soil Sci. Soc. Am. J.* 57, 1476–1479.
- Ray, C., Vogel, T., Dusek, J., 2004. Modeling depth-variant and domain-specific sorption and biodegradation in dual-permeability media. *J. Contam. Hydrol.* 70, 63–87.
- Roulier, S., Jarvis, N., 2003. Modeling macropore flow effects on pesticide leaching: inverse parameter estimation using microlysimeters. *J. Environ. Qual.* 32, 2341–2353.
- Roulier, S., Jarvis, N., 2003. Analysis of inverse procedures for estimating parameters controlling macropore flow and solute transport in the dual-permeability model MACRO. *Vadose Zone J.* 2, 349–357.
- Sabbah, I., Ball, W.P., Young, D.E., Bouwer, E.J., 2005. Misinterpretations in the modeling of contaminant desorption from environmental solids when equilibrium conditions are not fully understood. *Environ. Eng. Sci.* 22 (3), 350–366.

- Selim, H.M., Ma, L., Zhu, H., 1999. Predicting solute transport in soils: second-order two-site models. *Soil Sci. Soc. Am. J.* 63, 768–777.
- Šimůnek, J., Šejna, M., van Genuchten, M.T., 1998. The HYDRUS-1D Software Package for Simulating the One-Dimensional Movement of Water, Heat, and Multiple Solutes in Variably Saturated Media, Version 2.0, IGWMC-TPS-70. International Ground Water Modeling Center, Colorado School of Mines, Golden, Colorado. 202 pp.
- Šimůnek, J., Wendroth, O., Wypler, O., van Genuchten, M.T., 2001. Nonequilibrium water flow characterized from an upward infiltration experiment. *Eur. J. Soil Sci.* 52 (1), 13–24.
- Šimůnek, J., Jarvis, N.J., van Genuchten, M.T., Gärdenäs, A., 2003. Review and comparison of models for describing nonequilibrium and preferential flow and transport in the vadose zone. *J. Hydrol.* 272, 14–35.
- Skopp, J., Gardner, W.R., Tyler, E.J., 1981. Solute movement in structured soils: two-region model with small interaction. *Soil Sci. Soc. Am. J.* 45, 837–842.
- Smith, M.C., Shaw, D.R., Massey, J.H., Boyette, M., Kingerey, W., 2003. Using nonequilibrium thin-disc and batch equilibrium techniques to evaluate herbicide sorption. *J. Environ. Qual.* 32 (4), 1393–1404.
- Stehouwer, R.C., Dick, W.A., Traina, S.J., 1993. Characteristics of earthworm burrow lining affecting atrazine sorption. *J. Environ. Qual.* 22, 181–185.
- Stehouwer, R.C., Dick, W.A., Traina, S.J., 1994. Sorption and retention in vertically oriented earthworm and artificial burrows. *J. Environ. Qual.* 23, 286–292.
- Streck, T., Poletika, N.N., Jury, W.A., Farmer, W.J., 1995. Description of simazine transport with rate-limited, two-stage, linear and non-linear sorption. *Water Resour. Res.* 31, 811–822.
- U.S. Environmental Protection Agency (USEPA), 1993. Pesticides in Ground Water Database—A Compilation of Monitoring Studies: 1971–1991 National Summary. EPA 734-12-92-001. US EPA Office of Pesticide Programs, Washington, DC.
- Valocchi, A.J., 1985. Validity of the local equilibrium assumption for modeling sorbing solute transport through homogeneous soils. *Water Resour. Res.* 21, 808–820.
- Vanderborght, J., Gähwiler, P., Flühler, H., 2002. Identification of transport processes in soil cores using fluorescent tracers. *Soil Sci. Soc. Am. J.* 66, 774–787.
- Vanderborght, J., Kasteel, R., Vereecken, H., in press. Stochastic continuum transport equations for field-scale solute transport: overview of theoretical and experimental results. *Vadose Zone J.* 5 (2). doi:10.2136/vzj2005.0024.
- van Genuchten, M.T., 1980. A closed-form equation for predicting the hydraulic conductivity of unsaturated soils. *Soil Sci. Soc. Am. J.* 44, 892–898.
- van Genuchten, M.T., Wagenet, R.J., 1989. Two-site/two-region models for pesticide transport and degradation: theoretical development and analytical solutions. *Soil Sci. Soc. Am. J.* 53, 1303–1310.
- van Genuchten, M.T., Wierenga, P.J., 1976. Mass transfer studies in sorbing porous media: I. Analytical solutions. *Soil Sci. Soc. Am. J.* 40, 473–481.
- Veeh, R.H., Inskeep, W.P., Roe, F.L., Ferguson, A.H., 1994. Transport of chlorsulfuron through soil columns. *J. Environ. Qual.* 23, 542–549.
- Wagenet, R.J., Chen, W., 1998. Coupling sorption rate heterogeneity and physical nonequilibrium in soils. In: Selim, H.M., Ma, L. (Eds.), *Physical Nonequilibrium in Soils*. Ann Arbor Press, Chelsea, Michigan, pp. 1–36.
- Walker, A., Bromilow, R.H., Nicholls, P.H., Evans, A.A., Smith, V.J.R., 2002. Spatial variability in the degradation rates of isoproturon and chlorotoluron in a clay soil. *Weed Res.* 42, 39–44.
- Young, D.F., Ball, W.P., 2000. Column experimental design requirements for estimating model parameters from temporal moments under nonequilibrium conditions. *Adv. Water Resour.* 23 (5), 449–460.